bioRxiv preprint doi: https://doi.org/10.1101/498469; this version posted February 19, 2021. The copyright holder for this preprint (which was not certified by peer review) is the author/funder. All rights reserved. No reuse allowed without permission.

A novel mechanosensitive channel controls osmoregulation, differentiation and infectivity in *Trypanosoma cruzi.*

Dave, N[1]; Cetiner, U[2]; Arroyo, D[1]; Fonbuena, J[1]; Tiwari, M[1]; Barrera, P[3]; Lander, N[4]; Anishkin, A[2]; Sukharev, S[2] and Jimenez, V[1]*

[1]Department of Biological Science, College of Natural Sciences and Mathematics, California State University Fullerton; [2]Department of Biology, University of Maryland, College Park; [3] Departmento de Biología, Facultad de Ciencias Exactas y Naturales, Instituto de Histologia y Embriologia IHEM-CONICET, Facultad de Medicina, Universidad Nacional de Cuyo ; [4]Department of Biological Sciences, University of Cincinnati, Cincinnati, OH 45221.

Running title: A mechanosensitive channel in *Trypanosoma cruzi*

Address: [1]Department of Biological Sciences, College of Natural Sciences and Mathematics, California State University Fullerton. 800 N State College Blvd, McCarthy Hall 307, Fullerton, California 92831, U.S.A. Tel: 1-657-278-2477, Fax: 1-657-278-5390

e-mail: vjimenezortiz@fullerton.edu. *Correspondence and reprints.

Keywords: mechanosensation, calcium, osmoregulation, infectivity, CRISPR-Cas9, electrophysiology.

bioRxiv preprint doi: https://doi.org/10.1101/498469; this version posted February 19, 2021. The copyright holder for this preprint (which was not certified by peer review) is the author/funder. All rights reserved. No reuse allowed without permission.

Abstract (150 words)

Trypanosoma cruzi, the causative agent of Chagas disease, undergoes drastic morphological and biochemical modifications as it passes between hosts and transitions from extracellular to intracellular stages. The osmotic and mechanical aspects of these cellular transformations are not understood. Here we identify and characterize a novel mechanosensitive channel in T. *cruzi* (TcMscS) belonging to the superfamily of small conductance mechanosensitive channels (MscS). TcMscS is activated by membrane tension and forms a large pore permeable to anions, cations, and small osmolytes. The channel changes its location from the contractile vacuole complex in epimastigotes to the plasma membrane as the parasites develop into intracellular amastigotes. TcMscS knockout parasites show significant fitness defects, including increased cell volume, calcium dysregulation, impaired differentiation, and a dramatic decrease in infectivity. Our work provides mechanistic insights into components supporting pathogen adaptation inside the host thus opening the exploration of mechanosensation as a prerequisite of protozoan infectivity.

Introduction

Mechanosensation is a universal characteristic of all cells, from bacteria to mammals [1, 2]. Mechanosensitive channels (MSCs) act as sensors (transducers) and often as effectors of mechano-responses [3] and their activation leads to the movement of ions and small osmolytes, which mediates regulatory volume responses and/or triggers downstream signaling cascades [4-8]. Thus, mechanosensation allows cells to respond to stress conditions, maintaining relatively constant volume and macromolecular excluded volume of the cytoplasm. In eukaryotic organisms mechanosensation is involved in shear stress sensing and stem cell differentiation [9-11], regulating the fate of mesenchymatic tissues such as myoblasts and osteoblasts [12, 13] . Importantly, mechanical cues regulate the growth of normal and tumoral tissue [14-16], allowing for the invasion of the basal lamina and increasing the metastasis of tumors [17, 18]. MSCs in

bioRxiv preprint doi: https://doi.org/10.1101/498469; this version posted February 19, 2021. The copyright holder for this preprint (which was not certified by peer review) is the author/funder. All rights reserved. No reuse allowed without permission.

prokaryotes have been postulated to participate in quorum sensing, biofilm formation and regulation of virulence factors [19-22]. Protozoan pathogens, like trypanosomes and apicomplexans, are subjected to mechanical forces associated with shear stress in the bloodstream [23, 24], extravasation [25, 26] and invasion of tissues required for establishing persistent infection [27-31]. While it is clear that mechanical cues modulate the parasite life cycle and behavior, the molecular mechanism underlying sensing and triggering of the responses required for survival is unknown.

Trypanosoma cruzi, a flagellated protozoan, is the causative agent of Chagas disease, an endemic pathology in Latin America where millions are infected [32]. Recent studies indicate global changes in the epidemiology of the disease resulting in an increased incidence in non-endemic regions of the world [33, 34]. Similar to other protozoan pathogens [35-37], *T. cruzi* completes its life cycle by alternating between mammalian hosts and insect vectors. The parasite undergoes transitions between intracellular and extracellular forms, with periods of exposure to the environment. Drastic morphological and biochemical changes are required to ensure its survival in different environments [35]. *T. cruzi* epimastigotes replicate in the intestinal lumen of the insect vector where they endure osmotic concentrations of rectal material up to 1000 mOsm/Kg [38]. The infective metacyclic trypomastigotes are released into the environment with the feces of the vector and are able to penetrate the skin layers of a mammalian host, disseminating via blood circulation. The highly motile flagellated trypomastigotes survive shear stress in the bloodstream and then penetrate into host cells where, in the relatively constant cytoplasmic environment, they transform into the round non-motile intracellular amastigotes. The differentiation back to the extracellular infective trypomastigotes requires substantial volume and shape changes, cytoskeletal rearrangement, and elongation of the flagella. Additionally, *T. cruzi* has a strong tropism toward muscle cells, establishing chronic infection in cardiomyocytes and smooth muscle of the gastrointestinal track [39]. Parasite survival and growth in contractile tissues, as well as developmental transitions

bioRxiv preprint doi: https://doi.org/10.1101/498469; this version posted February 19, 2021. The copyright holder for this preprint (which was not certified by peer review) is the author/funder. All rights reserved. No reuse allowed without permission.

from intracellular to extracellular forms, pose significant mechanical challenges for the parasites [40].

Multiple signaling pathways are activated during osmotic responses, invasion and differentiation [41-44] including cAMP and calcium-dependent cascades [45, 46], but the primary molecular sensors triggering these processes have yet to be identified. *T. cruzi* regulates its volume via the Contractile Vacuole Complex (CVC) [47, 48] a specialized organelle also present in other protozoans like *Paramecium, Dictyostelium and Chamydomonas*, which experience substantial osmotic gradients across their plasma membranes. The CVC actively collects excessive fluid from the cytoplasm and ejects it through exocytic mechanisms [49]. In *Chlamydomonas*, yeast, and various higher plants, the mechanisms of volume adjustment, stress relief, biogenesis, and maintenance of intracellular organelles such as plastids are regulated by mechanosensitive channels [50-53]. These channels belonging to the prokaryotic MscS family, act as ubiquitous turgor regulators and osmolyte release valves in bacteria [4, 54, 55] and Archaea [56]. Currently, there is no information about such tension-stabilizing components in protozoan CVCs.

Here, we report the identification and functional characterization of a novel mechanosensitive channel in *T. cruzi* (TcMscS), which is a member of a MscS-related branch of channels present in Trypanosomatids [57]. The sequence analysis predicts a two-transmembrane domain architecture with a unique C-terminal domain. During the parasite life-cycle the channel is developmentally targeted to CVC in the extracelullar motile stages and to the plasma membrane in the intracellular amastigote stage. When expressed in bacterial spheroplasts the channel gates directly by membrane tension and shows a slight selectivity for anions. Gene targeting by CRISPR/Cas methods generated knockout and knockdown parasites that exhibit impaired growth and inability to robustly regulate cell volume. These parasites also show abnormal calcium regulation and a dramatic decrease in differentiation rate and infectivity, supporting the essential role of mechanosensitive channels in *T. cruzi*. Our results provide

bioRxiv preprint doi: https://doi.org/10.1101/498469; this version posted February 19, 2021. The copyright holder for this preprint (which was not certified by peer review) is the author/funder. All rights reserved. No reuse allowed without permission.

evidence that in trypanosomes, TcMscS and its homologs are involved in the sensing of mechanical forces generated during tissue migration and cell penetration, stabilizing pressure gradients and relieving mechanical membrane stresses during cell volume regulation and developmental transitions.

Results

Sequence analysis and structural features of TcMscS predicted by homology model

Analysis of Trypanosoma databases (tritrypdb.org) revealed the presence of a putative MscS-like ion channel (TcCLB.504171.40) in the Esmeraldo-like haplotype of the *T. cruzi* CL Brener strain genome (TcMscS). This channel shares 94.5% identity at the protein level with the non Esmeraldo-like allele (TcCLB.509795.40) and has homologues in *T. brucei* (Tb427.10.9030) and *Leishmania major* (LmjF.36.5770), sharing 66% and 58% identity, respectively (Fig. 1A). Overall sequence conservation between TcMscS and *E. coli* MscS is low (25.4%), but the percentage of identity increases to 38% in the core comprising transmembrane helices TM2 and TM3. The full alignment of four protozoan and two bacterial sequences is shown in supplemental Figure S1. The ORF of TcMscS is 498 nucleotides, predicting a protein of 165 amino acids (17.8 kDa). Assuming that TcMscS follows the same oligomerization pattern as *E. coli* MscS [58], it is expected to form a heptamer. The refined consensus homology model based on several structure prediction servers (Fig. 1B) indicates the presence of two transmembrane domains, with a preceding N-terminal segment (red). The chain continues as TM2 (gold), crosses the membrane, makes a short loop and returns back as pore-forming TM3 (green). The gate of TcMscS is predicted to be formed by the ring of F64, which is in the precise homologous position with the gate-forming L109 of EcMscS.

The labeling of TcMscS helices in Fig. 1 matches the homologous segments of prokaryotic MscS. Because the TM1 segment in TcMscS is too short to cross the membrane, it is modeled in the conformation attached to the inner surface of the membrane (N1). The beta

bioRxiv preprint doi: https://doi.org/10.1101/498469; this version posted February 19, 2021. The copyright holder for this preprint (which was not certified by peer review) is the author/funder. All rights reserved. No reuse allowed without permission.

domain (cyan) is the last segment that aligns with EcMscS. The complete TcMscS homology model, which includes the bundled C-terminal segment, is shown in the predicted closed and open conformations (Fig. 1C). In addition to the F64 constriction (main gate), the beta domain that follows TM3 is predicted to bear a second hydrophobic constriction (Fig. 1C top panel, pink residues). This hypothetical C-terminal (cytoplasmic) gate formed by L97 (Fig. 1C, bottom panel, yellow residues) is narrower than the cage constriction present in *E. coli* MscS. The full model also shows the predicted opening transition that widens both gates. The overall displacement and tilting of TM3 helices on opening transition is modeled to increase the main gate radius from 3.9 to 6.5 Å accompanied by an in-plane area expansion of the protein by approximately 5.0 nm^2. The *de novo* modeled flexible linkers lead to the C-terminal amphipathic helical domains hypothesized to form a coiled-coil bundle (blue), similar to what was observed in the crystal structures of MscL [59], another type of bacterial MS channel. The linkers and bundle might serve as a pre-filter to exclude larger osmolytes from occluding the pore. Overall, the structural model prediction supports the formation of a hepatmeric channel with a higher degree of conservation in the pore forming region and some key differences in the C-terminal segment, which is unique to TcMscS.

Electrophysiological characteristics of TcMscS

To evaluate the functional properties of TcMscS, electrophysiological recordings were performed in *E. coli* giant spheroplasts (MJF641 Δ7 strain) expressing the channel. Single-channel currents were measured at low protein expression, with 1-3 channels per patch. Fig. 2A shows typical single-channel traces recorded under 110 mmHg pressure steps at +40 and -40 mV pipette voltages. The current amplitude of 12 pA translates to 0.40±0.02 nS conductance (n=11). The I-V curve for TcMscS obtained under symmetric electrolyte conditions (200 mM KCl) is linear (Fig 2B, black symbols), in contrast to EcMscS which shows a visible rectification [4, 60]. After a perfusion of buffer containing 425 mM KCl in the bath (Fig 2B, red symbols), the I-V curve changes its slope and the x-intercept reproducibly shifts to -4.3 ±0.4mV (n=4).

bioRxiv preprint doi: https://doi.org/10.1101/498469; this version posted February 19, 2021. The copyright holder for this preprint (which was not certified by peer review) is the author/funder. All rights reserved. No reuse allowed without permission.

According to the Goldman equation, under a given ionic gradient the reversal potential of -4.3 mV corresponds to a P_{Cl-}/P_{K+} of 1.6, signifying that the channel passes about 3 Cl^- ions per 2 K^+ ions, i.e., it shows a slight anionic preference.

To explore whether the channel is permeable to Ca^{2+}, we filled the pipette with 100 mM Ca gluconate (supplemented with 20 mM $CaCl_2$ to ensure the silver chloride electrode works) and recorded unitary currents under asymmetric conditions with the standard 200 KCl buffer in the bath. Under positive pipette voltage (+30 mV), we recorded 12 ± 1 pA currents contributed by the inward flux of Ca^{2+} and outward flux of Cl^- (Fig. 2C). We then thoroughly perfused the bath solution with 100 mM Ca gluconate making Ca^{2+} the dominant permeable ion at this polarity. The amplitude of current dropped to 0.9 ±0.5 pA (n=3), translating into a 30 pS conductance (Fig. 2D). Our previous data [60] indicated that the unitary conductance of EcMscS scales linearly with the bulk conductivity of monovalent salt surrounding the channel. More recently, EcMscS was shown to be highly permeable to Ca^{2+} [7], its unitary conductance in 100 mM $CaCl_2$ is about a half (0.5 nS) of the conductance in equimolar KCl (1.1 nS). In our experiment with TcMscS, the 400 pS unitary conductance in symmetric 200 mM KCl (24.1 mS/cm) drops to 30 pS in 120 mM Ca gluconate (4.64 mS/cm). The 5.2 fold drop in bulk conductivity resulted in a 13 fold decrease in unitary conductance, strongly suggesting that Ca^{2+} is still permeable through TcMscS, although at a lower level compared to monovalents. Interestingly, the TcMscS never opened at negative pipette potentials in the presence of high Ca^{2+}.

Figure 2E shows two population currents recorded at + 30 or -30 mV in the pipette with identical ramp stimuli. The appearance of channels is essentially identical at two opposite voltages. The closing rate appears extremely slow as some channels remain open up to about 10 s after the stimulus ends.

To define the gating characteristics of TcMscS we analyzed the responses under pressure ramps and normalized the traces to saturating current to find the open probability and

bioRxiv preprint doi: https://doi.org/10.1101/498469; this version posted February 19, 2021. The copyright holder for this preprint (which was not certified by peer review) is the author/funder. All rights reserved. No reuse allowed without permission.

statistically assessed midpoint pressure required for activation (Fig. 2F). With EcMscS as a reference for known tension midpoint, we estimated the midpoint tension for TcMscS. EcMscS showed its half-activation pressure at 90 ± 3 mmHg (Fig. 2F, black symbols, n=54). TcMscS, had its pressure midpoint at 145 ± 20 mmHg (Fig. 2F, blue symbols n=11). Given that EcMscS activates in *E. coli* spheroplasts at 7.8 mN/m [61], we concluded that the midpoint of TcMscS activation is 12.6 mN/m. Although both channels start opening at approximately the same pressure (tension), the activation curve for TcMscS is shallower. Fitting the initial slopes of logarithmic Po/Pc plots (panel F, inset) using the two-state Boltzmann equation [62] gave estimates of the energies and in-plane area changes associated with gating. Gating of TcMscS was characterized by a 3 nm^2 effective expansion of the protein, whereas the slope of EcMscS curve produced a 10.5 nm^2 lateral expansion, consistent with models presented in Figure 1 and previous work by Anishkin et al [63].

These results unequivocally demonstrate that TcMscS is a mechanosensitive channel with functional characteristics comparable to the ones observed in bacterial MscS channels. It opens at sub-lytic tensions and, based on conductance, forms a ~ 12 Å pore, which is essentially non-selective and capable of passing both anions and cations, including calcium, and possibly organic osmolytes such as betaine and other small amino acids.

TcMscS expression and localization

To determine TcMscS localization, we generated polyclonal antibodies against the recombinant protein (*Supplementary materials and methods*). By immunofluorescence analysis (Fig. 3A) we found TcMscS mostly localized in the bladder of the contractile vacuole complex (CVC) of epimastigotes (Fig. 3A) and trypomastigotes (Fig. 3B). In epimastigotes, TcMscS colocalizes with VAMP7, another CVC protein [64, 65] (Fig. 4A), and partially colocalizes with actin (Fig. 4B). Interestingly, no colocalization with tubulin was observed (Fig. 4C). In trypomastigotes, TcMscS is found in the CVC bladder and is also distributed along the flagellum and the cell body (Fig. 3B), but shows no co-localization with the membrane marker SSP-1 (Fig.

bioRxiv preprint doi: https://doi.org/10.1101/498469; this version posted February 19, 2021. The copyright holder for this preprint (which was not certified by peer review) is the author/funder. All rights reserved. No reuse allowed without permission.

4D). In intracellular amastigotes, TcMscS has a peripheral localization and no labeling was detected in the CVC (Fig. 3C). Colocalization with the amastigote membrane marker SSP-4 shows a clear overlap of the labeling (Fig.4E), indicating the translocation of TcMscS to the plasma membrane. The differential localization in the extracellular versus intracellular stages suggest that TcMscS could be playing different physiological roles in response to developmental and/or environmental cues. This hypothesis is reinforced by our data showing higher expression of TcMscS in epimastigotes compared with amastigotes and trypomastigotes, at the mRNA (Fig. 3D) and protein levels (Fig. 3E). Epimastigotes at the stationary phase of growth have a significantly lower amount of transcript compared with parasites in exponential growth (Fig. 3D), but no evident difference in the amount of protein was observed by Western blot analysis (data not shown).

TcMscS gene targeting by CRISPR-Cas9

To establish the physiological role of TcMscS in the parasites, we targeted the gene using the CRISPR-Cas9 system with (Fig. 5) or without DNA donor for gene replacement (Fig. S2). When we transfected the parasites with the Cas9/pTREX-n vector containing sgRNA2 (Table S1) targeting *TcMscS* without DNA donor, we observed a single nucleotide deletion (*del*177G), resulting in a frame shift and a premature stop codon (Fig 5A, top panel). These results were confirmed by genomic DNA sequencing in multiple independent samples. The truncated protein at amino acid 79 is not expected to be functional (Fig 5A, bottom panel) since the C-terminal end is absent. In these parasites, the transcript for TcMscS was still detected, although at significantly lower level compared with control parasites only expressing Cas9 and a scrambled sgRNA (Fig. 5C). Based on the level of mRNA and the detection of residual protein by Western-blot analysis (Fig. S3, A and B) it is possible that we are only targeting one of the alleles of the gene and we considered this strain a knockdown (TcMscS-KD). Importantly, the growth of TcMscS-KD epimastigotes is significantly reduced (Fig. S2 B, blue line) when compared to WT (Fig. S2 B, black line) and Cas9-scr controls (Fig. S2 B, red line). The

bioRxiv preprint doi: https://doi.org/10.1101/498469; this version posted February 19, 2021. The copyright holder for this preprint (which was not certified by peer review) is the author/funder. All rights reserved. No reuse allowed without permission.

parasites show abnormal morphology, with rounded bodies and formation of rosettes (Fig. S2 D, bottom panel).

To completely abolish the expression of TcMscS, we co-transfected the parasites with sgRNA2-Cas9/pTREX-n vector plus a donor DNA cassette for homologous-directed repair (Fig. 5A). Genomic DNA analysis by PCR shows the absence of the *TcMscS* gene and the correct insertion of the blasticidin resistance cassette (Fig. 5B). No transcript was detected in epimastigotes (Fig. 5D) or trypomastigotes (Fig. S3, C). These results were confirmed by Western blot analysis (Fig. S3, A) and immunofluorescence (Fig. 5E), demonstrating the successful knockout of *TcMscS* (TcMscS-KO).

As expected, the growth rate of TcMscS-KO epimastigotes was significantly reduced (Fig. 5C, green line) and was lower than in TcMscS-KD parasites (Fig. 5C, blue line). The decrease in growth is accompanied by a marked reduction in motility (Suppl. Video 1 and 2), showing that the ablation of the channel has a negative effect on parasite fitness. To verify the specificity of the phenotype, we complemented the KO strains with the overexpression vector pTREX carrying a copy of TcMscS C-terminally tagged with myc. We successfully expressed the tagged construct (Fig. S4 A, C1 and C2), but as expected based on our previous data, the overexpression has a detrimental effect on the cells. This is in agreement with previous reports of porin and porin-like overexpression toxicity [66, 67]. The cell growth was not recovered (Fig. S4 B) and the epimastigotes showed abnormal morphology (Fig. S4 C). We then complemented the TcMscS-KO strain with a copy of the *T. brucei* ortholog TbMscS (Fig. S4 A and B, C3) and we were able to partially revert the cell growth phenotype, indicating some function conservation of the channel in other trypanosomatids.

TcMscS regulates parasites osmotic stress responses

To evaluate the role of TcMscS in cell volume regulation we exposed the parasites to osmotic changes and followed the variations in absorbance over time as an indicator of variations in cell volume. Under hypoosmotic conditions of 115 mOsm/L (Fig. 6A) TcMscS-KD

bioRxiv preprint doi: https://doi.org/10.1101/498469; this version posted February 19, 2021. The copyright holder for this preprint (which was not certified by peer review) is the author/funder. All rights reserved. No reuse allowed without permission.

and KO epimastigotes experienced a maximum change in volume of about 38% compared with 23-25% in the controls (Table S2, Peak and Fig. 6B). When we analyzed the rate of recovery between 200-400 s, no significant difference was observed in the slope values, except for TcMscS-KO that had a slightly higher value. Nevertheless, KD and KO parasites do not regain their normal volume after 600 s, showing a remaining volume change of about 20% (Table S2, Final volume, Fig. 6C).

These results indicate that TcMscS, similar to other MscS channels, activates in response to increased membrane tension which results in redistribution of osmolytes and thus prevents excessive cell swelling. However, TcMscS-KD and KO parasites under hypoosmotic stress do not lose control of their volume completely, suggesting that TcMscS must act in conjunction with other mechanisms to orchestrate effective regulatory volume decrease responses.

Upon hyperosmotic stress of 650 mOsm/L (Fig. 6D), a similar phenotype was observed, with TcMscS-KD and TcMscS-KO parasite reducing their volumes by about 20%, compared with 12-15% in the controls (Table S3, Peak; Fig. 6E). As previously described [68], epimastigotes under hyperosmotic conditions do not regain normal volume, and parasites lacking TcMscS remained significantly more shrunken compared to controls (Fig. 6F), showing that TcMscS is required for regaining normal cell volume following hyperosmotic stress. We evaluated whether TcMscS localization changes upon osmotic stress and observed no differences in parasites under iso-, hypo- or hyperosmotic conditions at different time points (Fig. S5). It should be noted that TcMscS-KD and KO epimastigotes under isosmotic conditions show a cell volume about 36-38% higher than normal when compared with WT and Cas9 controls (Fig. S6). This significant difference underscores the role of TcMscS in the regulation of cell volume under normotonic conditions.

TcMscS-KO causes cytosolic calcium dysregulation

bioRxiv preprint doi: https://doi.org/10.1101/498469; this version posted February 19, 2021. The copyright holder for this preprint (which was not certified by peer review) is the author/funder. All rights reserved. No reuse allowed without permission.

TcMscS localization in the CVC and our electrophysiology data showing the permeation of calcium through the channel lead us to evaluate the cytosolic calcium level in the KO parasites. WT epimastigotes loaded with Fura 2-AM showed a baseline cytosolic Ca^{2+} of 102 ± 4 nM (n=9) and a robust increase upon addition of 1.8 mM extracellular $CaCl_2$ (Fig. 7 A and B, black line) reaching 208 ± 8 nM 100 s post-stimulation. In contrast, TcMscS-KO had a lower baseline Ca^{2+} of 81 ± 4 nM (n= 8) and a lower increase post-addition (Fig. 7 A and B, green line). The increase in cytosolic free Ca^{2+} can be caused by release of the ion from intracellular stores and/or by uptake from the extracellular media. To evaluate whether the impairment of the KO was due to a reduced uptake, we treated the cells with Bay K8644, a known activator of voltage gated calcium channels (VGCC). These channels have been postulated as the main permeation pathway for extracellular Ca^{2+} in *T. cruzi* [69] but other reports have indicated its presence in the CVC [64]. When we stimulate the cells in the presence of Bay K (Fig. 7 C and D), WT parasites show a dramatic increase in cytosolic Ca^{2+}, 10 fold higher than in non-pretreated cells (Fig. 7 A and C, black lines). TcMscS-KO exhibited an increase in cytosolic Ca^{2+} compared with non-Bay K conditions (Fig. 7 A and C, green lines), but the response was significantly lower than in WT (Fig. 7 D post-Bay K). Collectively, these results indicate the role of TcMscS in regulating the cytosolic Ca^{2+} dynamic on the parasites, probably by controlling intracellular stores such as the CVC. The lack of adequate Ca^{2+} homeostasis can severely impact cell motility and infectivity.

TcMscS-KO impairs parasite differentiation and infectivity

To elucidate the role of TcMscS in *T. cruzi's* infectivity, we first evaluated the localization of the channel in metacyclic trypomastigotes (Fig. 8A). Similar to tissue-derived trypomastigotes, TcMscS is localized in the CVC bladder of the metacyclic forms, but also along the cell body, on the flagellar attachment zone region. The differentiation to metacyclic trypomastigotes *in vitro* is severely impaired in TcMscS-KO parasites, producing only 0.38% versus 6% obtained from WT epimastigotes after 72h of incubation in TAU media (Fig. 8B) [70].

bioRxiv preprint doi: https://doi.org/10.1101/498469; this version posted February 19, 2021. The copyright holder for this preprint (which was not certified by peer review) is the author/funder. All rights reserved. No reuse allowed without permission.

We were able to infect mammalian cells with TcMscS-KO metacyclic trypomastigotes and obtained tissue culture derived trypomastigotes. The infective capacity of these parasites was not affected at early time points post-infection (Table S4) but did show a significant decrease in the production of intracellular amastigotes at 48 h post-infection (Fig. 8C and E; Table S4). These results confirm a defect in the capacity of the TcMscS-KO to replicate intracellularly. Quantification of extracellular trypomastigotes collected from the tissue culture supernatant shows a significant decrease in the number of TcMscS-KO parasites able to successfully differentiate into bloodstream trypomastigotes and egress from the cells (Fig. 8D). At 6 days post infection, TcMscS-KO produced a total of 5.2 x 10^6 extracellular parasites, almost one order of magnitude lower than the amount produced by the Cas9-scr strain and WT parasites (Table S5).

In summary, the ablation of *TcMscS* results in loss of parasite fitness, impairing osmotic regulation, motility, calcium homeostasis, differentiation and cell infection capacity. The multiple phenotypic defects observed in TcMscS-KO parasites indicate that the physiological roles of this mechanosensitive channel have expanded beyond the primarily osmotic compensation reported for its bacterial ancestor EcMscS.

Discussion

Propagation of *T. cruzi* involves alternating between mammalian and insect hosts; a life-history strategy that imposes significant mechanical demands on the parasite. This complex life cycle requires protective mechanisms and a strong differentiation potential that drives massive cell remodeling. The presence of TcMscS homologs in *Toxoplasma gondii*, *Plasmodium falciparum* and *Entamoeba histolytica* suggests a conserved function for these channels in other protozoan parasites [57]. Understanding their role as molecular transducers as well as likely effectors of mechanical cues throughout the parasites life cycle can provide new information about the role of physical and osmotic forces in the mechanisms regulating infectivity.

bioRxiv preprint doi: https://doi.org/10.1101/498469; this version posted February 19, 2021. The copyright holder for this preprint (which was not certified by peer review) is the author/funder. All rights reserved. No reuse allowed without permission.

In this work we identify and present a functional characterization of the first MscS-like mechanosensitive channel in protozoan pathogens. TcMscS, a novel mechanosensitive channel found in *T. cruzi*, is required for growth, calcium homeostasis, differentiation and infectivity. The channel plays special roles in balancing osmotic and/or contractile forces in a stage- and location-specific manner. TcMscS belongs to the MscS superfamily and is structurally and functionally similar to the well characterized EcMscS [60]. MscS-like channels are a highly diverse group of proteins [71] found in Archaea [56], fungi [72-74], protozoans [75-77] and plants [51, 52, 78, 79], but not found in metazoans. The evolutionary origin of MscS-like channels can be traced to a common ancestor that was maintained across lineages as a protective mechanism against osmotic stress [80]. Beyond their primary role in volume regulation, these channels are also implicated in amino acid transport [81, 82] calcium homeostasis [73, 74, 83], and organelle biogenesis and maintenance [51-53, 78, 84, 85], highlighting the diversification of functions for this protein family over its evolutionary history [71, 86].

Expression in □7 *E. coli* spheroplasts provided a clean experimental system to study activation by tension and single-channel properties of TcMscS. The linear non-rectifying conductance of the channel is approximately half of the conductance of EcMscS [60]. Similar to other MscS-like channels, TcMscS has a slight selectivity towards anions, but also shows measurable permability to calcium.

The size of the pore appears be sufficient for permeation of small organic osmolytes. In *T. cruzi*, regulatory volume decrease is driven primarily by efflux of amino acids and requires fluctuations in intracellular calcium [87]. Given the localization in the CVC and the non-selective nature of TcMscS, this channel could be a permeation pathway for amino acids and calcium required for cell volume regulation. An activation midpoint near 12 mN/m determined in bacterial spheroplasts suggests that the channel becomes fully active at tensions approaching the lytic limit, and thus it fulfills the role of a stress-releaving emergency valve, permitting the

bioRxiv preprint doi: https://doi.org/10.1101/498469; this version posted February 19, 2021. The copyright holder for this preprint (which was not certified by peer review) is the author/funder. All rights reserved. No reuse allowed without permission.

equilibration of osmolytes. TcMscS activities recorded in a heterologous expression system strongly suggest that the channel is gated directly by tension in the lipid bilayer without the need for cytoskeleton or other Tc-specific components. The ramp responses of TcMscS populations indicate a slow closing rate that allows the channel to remain open for a longer period, thus relieving the hypoosmotic stress more completely.

The channel has a novel 2TM topology (Fig. 1) and shows substantial homology with *E. coli* MscS only in the TM3 and beta domain region. Common to other tension-activated channels [88], TcMscS is predicted to have a short amphipathic N-terminal helix attached to the inner leaflet of the membrane. TcMscS has a completely unique C-terminal domain predicted to fulfill the function of pre-filter at the cytoplasmic entrance.

In most cell types, MscS channels are localized in the plasma membrane, but they are also found in internal organelles including the ER [73], contractile vacuole [50, 89-91] and plastids [53, 77] . In *T. cruzi*, TcMscS shows a differential localization in the extracellular versus intracellular stages. In epimastigotes, the channel has a defined intracellular localization in the bladder of the contractile vacuole and partially colocalizes with VAMP-7 and actin. There are no previous reports of actin associated to the bladder of the CVC, but we have shown the expression of myosin heavy chains V1 and V2 [64] suggesting the presence of a contractile machinery that might contribute to the periodic discharge of the organelle, similar to what has been described in *D. discoideum and Paramecium* [90, 92]. In tissue-derived bloodstream and *in vitro*-differentiated metacyclic trypomastigotes, TcMscS localization is expanded beyond the CVC to include the cell body and part of the flagellum. This suggests that the channel could be sensing changes in tension during flagellar beating.

The role of CVC as a key regulator of the cell volume in *T. cruzi* has been extensively characterized [47] and the presence of a mechanosensitive channel in CVC points to necessity of curbing excessive tensions to protect the organelle from osmotic lysis. Proteomic and functional analysis has shown the presence of numerous proteins involved in volume

bioRxiv preprint doi: https://doi.org/10.1101/498469; this version posted February 19, 2021. The copyright holder for this preprint (which was not certified by peer review) is the author/funder. All rights reserved. No reuse allowed without permission.

compensation [64], but no sensor of the osmotic state has been identified. We propose that TcMscS is activated upon excessive filling of the bladder, similar to what has been proposed in other protists [48, 92, 93]. If the normal exocytotic release of the bladder content fails to relieve pressure, the channel activation may release the content back to the cytoplasm to preserve the integrity of the CVC.

The peripheral localization of TcMscS in amastigotes deserves further consideration. Intracellular stages develop free in the cytosol under osmotically stable conditions, establishing persistent infection predominantly in muscle cells where contractility generates periodic stress [40]. It is known that *T. cruzi* infection causes extensive cytoskeletal remodelling and the amastigotes are not protected by a parasitophorous vacuole, thus, they can be mechanically perturbed [94-97]. At this stage, TcMscS main role could be detecting changes in tension and shear stress elicited by host cell contraction. Alternatively, these results can be interpreted considering a simple topological factor: the spherical amastigotes would be more sensitive to osmotic downshock, whereas elongated forms have room for swelling and are better protected by a stronger cytoskeleton, explaining the change of TcMscS localization in amastigotes. In addition, the channel may be facilitating cell volume adjustments in the course of active cell reshaping during differentiation to trypomastigotes, which are preparing to exit the cells.

TcMscS expression is developmentally regulated, with higher levels in epimastigotes at the exponential phase of growth. Changes in expression and localization of the channel could be responding to stage-specific cues, as well as external conditions, allowing the parasites to successfully transition through their developmental cycle. To test this hypothesis, we used CRISPR/Cas9 [98] to target TcMscS in the parasites and produced two strains with similar characteristics but different level of phenotypic defects. Neither the reduction (KD) or the elimination (KO) of the gene resulted in a lethal phenotype, but both cell lines showed a detectable increase in cell volume, a significant reduction in their extracellular and intracellular replication rates and impaired ability to produce metacyclic and bloodstream trypomastigotes,

bioRxiv preprint doi: https://doi.org/10.1101/498469; this version posted February 19, 2021. The copyright holder for this preprint (which was not certified by peer review) is the author/funder. All rights reserved. No reuse allowed without permission.

decreasing the infectivity of the parasites. The role of mechanical cues in differentiation has been demonstrated in several cell types including mesenchymal stem cells [11], osteoclasts [99] and neurons[14] where TRPV and PIEZO 1 mechanosensitive channels activity regulates developmental transitions [13, 100] and axonal growth [14]. Here, we provide the first evidence that mechanosensation mediated by TcMscS influences the developmental transition from non-infective to infective forms in *T. cruzi,* supporting the role of these channels in cell differentiation.

TcMscS-KO strains exhibited reduced motility and loss of infectivity. This is consistent with recent studies showing that motility is necessary for virulence in *T. brucei* [101]. In trypanosomatids, flagellar beating and motility are regulated by Ca^{2+} transients generated in a directional manner along the flagellum [102].The generation of Ca^{2+} waves linked to the activation of mechanosensitive channels has been demonstrated in *Chlamydomonas* [103], tubular kidney cells [104, 105], lung epithelial lining [106] and bone cells [11]. In *T. brucei*, a putative Ca^{2+} channel has been shown to be essential for flagellar attachment and cell viability [107] suggesting that Ca^{2+} influx is required for normal function. In *T. cruzi*, an ortholog of this Ca^{2+} channel has been identified in the CVC [64]. Our results show a dysregulation in the Ca^{2+} responses of TcMscS-KO, both at rest and after stimulation with calcium and Bay K. TcMscS seems to participate in the modulation of Ca^{2+} dynamics either directly, by regulating calcium release from intracellular stores like the CVC [48, 108] or indirectly by changing the ionic environment and membrane potential that control the activation of voltage-gated calcium channels. This association between the role of CVC in calcium regulation and TcMscS could explain the observed defects in motility and infectivity (Suppl. videos 1 and 2).

In yeast and plants MscS-like channels localized intracellularly regulate cytosolic Ca^{2+} oscillations required for organelle homeostasis and volume regulation [51, 73, 74, 77, 79, 84], supporting our hypothesis that TcMscS could be playing similar roles in *T. cruzi*.

As expected, the mutant parasites also showed a decreased ability to control cell volume both under stress and normal conditions, confirming the role of TcMscS in osmotic homeostasis.

bioRxiv preprint doi: https://doi.org/10.1101/498469; this version posted February 19, 2021. The copyright holder for this preprint (which was not certified by peer review) is the author/funder. All rights reserved. No reuse allowed without permission.

The compromised RVD observed in the knockout parasites suggest that other channels or transporters could be involved in the compensatory responses. This has been well documented in bacteria, where double knockout of MscS and MscL are required to elicit a defect in osmoregulation. In *T. cruzi*, bioinformatic analysis shows the presence of genes encoding for putative Piezo-like [57] and TRP-like channels[109]. Our RNAseq analysis of TcMscS-KO parasites do not show a significant change in the expression of those genes (data not shown). These results do not rule out the possibility of an increase in channel activity, independent of the mRNA expression level.

In summary, we have identified and functionally characterized the first mechanosensitive channel in trypanosomatids. TcMscS resembles bacterial MscS in its core, but lacks the first transmembrane helix and has a modified cytoplasmic domain. Beyond its canonical role in osmoregulation, the channel participates in calcium homeostasis and its ablation affects the capacity of the cells to proliferate, move, differentiate, and infect host cells. Our work opens new avenues to explore the connection between sensing of physical stimuli and the activation of signaling pathways implicated in differentiation and host-parasite interaction. It also identifies new effectors that bridge sensing of external cues and the factors that drive stage transitions of protozoans in a host-specific manner. Additionally, these types of channels are not present in mammalian cells, offering potential as novel and selective targets for drug development.

Material and Methods

Electrophysiological recordings of TcMscS

For electrophysiological studies in *E. coli* giant spheroplasts we used a N-terminally 6-His tagged version of *TcMscS* cloned into the expression plasmid pQE80 (Qiagen) with restriction sites BamHI and HindIII. TcMscS was expressed in the MJF641 (aka Δ7) strain devoid of seven endogenous MS channel genes [110]. The strain was a gift from Dr. Ian Booth (University of Aberdeen, UK). Competent MJF641 cells were transformed, selected overnight for

bioRxiv preprint doi: https://doi.org/10.1101/498469; this version posted February 19, 2021. The copyright holder for this preprint (which was not certified by peer review) is the author/funder. All rights reserved. No reuse allowed without permission.

transformants on plates with 100 □g/ml ampicillin, and used immediately for spheroplast preparation. Spheroplast preparation was done following standard protocols [111]. Briefly, 3 ml of the colony-derived culture was transferred into 27 ml of LB containing 0.06 mg/ml cephalexin to block septation. After 1.5-2 hours of incubation, 1 mM IPTG was added to induce protein expression for 20 min. The filaments were transferred into a hypertonic buffer containing 1 M sucrose and subjected to digestion by lysozyme (0.2 mg/ml) in the presence of 5 mM EDTA resulting in spheres of 3-7 µm in diameter. The reaction was terminated by adding 20 mM Mg^{2+}. Spheroplasts were separated from the rest of the reaction mixture by sedimentation through a one-step sucrose gradient.

Recording conditions and protocols

Borosilicate glass (Drummond 2-000-100) pipets with tips 1-1.3 µm in diameter (bubble number 4.9-5.1) were used to form tight seals with the inner membrane. The tension-activated channel activities were recorded in excised inside-out patches. In most experiments the pipette and bath solution were symmetrical (200 mM KCl, 50 mM $MgCl_2$, 5 mM $CaCl_2$, 5 mM HEPES, pH 7.4). The bath solution was supplemented with 400 mM sucrose to osmotically balance the spheroplasts. An asymmetric configuration 425 mM /200 mM KCl (bath/pipette) was used to determine the channel's anion/cation selectivity.

Calcium permeability was measured with a pipette solution containing 100 mM Ca gluconate, 20 mM CaCl2, 5 mM Hepes, pH 7.2 and bath solution containing only 100 mM Ca gluconate. The activities of TcMscS were recorded under a pressure ramp 0 to -200 mm Hg, at +30 mV or -30 mV voltage in the pipette. Traces were recorded using Clampex 10.3 software (MDS Analytical Technologies). Programmed mechanical stimuli were delivered using a modified high-speed pressure clamp apparatus (HSPC-1; ALA Scientific Instruments).

Cell culture

Wild-type Y-strain (WT) epimastigotes were cultured in Liver Infusion Tryptose

bioRxiv preprint doi: https://doi.org/10.1101/498469; this version posted February 19, 2021. The copyright holder for this preprint (which was not certified by peer review) is the author/funder. All rights reserved. No reuse allowed without permission.

medium (LIT) as previously described [112]. Epimastigotes transfected with pTREX constructs including Cas9scr and TcMscS mutants (TcMscS-KD and TcMscS-KO) were cultured in LIT media supplemented with 10% FBS-HI and selection antibiotics (250 µg/mL of geneticin (G-418) and 15 µg/ml blasticidin) [98].

Tissue-derived bloodstream trypomastigotes and amastigotes were obtained as previously described [43]. Human foreskin fibroblast (HFF) and HEK-293 cells were cultured in High Glucose Dulbecco's Modified Eagles Media (HG-DMEM) supplemented with 100 units/mL of penicillin, 100 µg/mL of streptomycin, 0.2% of amphotericin B, and 10% FBS-HI, and incubated at 37 °C with 5 % CO2.

In Vitro Metacyclogenesis

Differentiation to metacyclic trypomastigote forms was induced under chemically defined conditions using triatomine artificial urine (TAU) medium as described [70]. Epimastigotes at 4 days of growth were collected by centrifugation at 1600 × g for 10 minutes, washed once in phosphate buffered saline solution (PBS) pH 7.4, resuspended in TAU media and incubated 2 hours at 28 °C. The supernatant was collected and resuspended in TAU with amino acids (TAU3AAG), incubated for up to 7 days at 28°C, collected by centrifugation resuspended in 5 mL of Dulbecco's Modified Eagles Media (DMEM) supplemented with 20% fresh FBS to eliminate residual epimastigotes.

In vitro infection assays

HEK-293 cells were plated onto coverlips in 12 well plates (1,000 cells/well) and incubated in supplemented HG-DMEM overnight at 37°C with 5% CO_2. Infections were performed at a multiplicity of infection (MOI) of 25:1 with either WT, Cas9scr or TcMscS mutant trypomastigotes. After 6 hours, the cells were washed 3 times with Hank's media and fresh DMEM was added. Coverslips were fixed in 4% paraformaldehyde-PBS at 6, 24 and 48 h, stained with DAPI (5 µg/ml) and mounted in Fluoromont media for quantification of intracellular

bioRxiv preprint doi: https://doi.org/10.1101/498469; this version posted February 19, 2021. The copyright holder for this preprint (which was not certified by peer review) is the author/funder. All rights reserved. No reuse allowed without permission.

parasites or processed for immunofluorescence. Immunofluorescence assays were performed to verify expression of Cas9-GFP and TcMscS in intracellular amastigote forms. Cells were incubated with anti-TcMscS (1:100) antibody and anti-GFP rabbit serum (Thermo Fisher Scientific, Inc.) (1:3,000) antibodies. Pictures were acquired in an Olympus IX83 microscope and processed with CellSens Dimension. All infection quantifications were done in 4 coverslips per experiment, in 3 or more independent experiments. At least 100 host cells were quantified per coverslip. The number of host cells vs. parasites was compared by a two-way ANOVA.

Quantification of extracellular trypomastigotes

The amount of infective forms released from HEK-293 cells infected at a MOI of 25:1 was evaluated by collecting the supernatant of the cultures at days 4, 5 and 6 post-infection. To eliminate possible contamination with detached cells, the supernatant was first centrifuged at 300 x g for 5 minutes. The supernatant containing trypomastigotes was then centrifuged at 1,600 x g for 5 minutes and resuspended in 1 ml of DMEM. The cells were counted in a Z2 Beckman Coulter cell counter. All quantifications were done in triplicate for 3 independent experiments.

TcMscS mutant generation by CRISPR/Cas9

Two strategies were developed to generate TcMscS-KD and TcMscS-KO mutants using the CRISPR/Cas9 one-vector system [98]. WT epimastigotes were transfected only with sgRNA/Cas9/pTREXn vector containing a sgRNA targeting *TcMscS*. Alternatively, the single vector containing TcMscS-sgRNA was co-transfected with a donor DNA to induce double strand break repair by homologous recombination, carrying a blasticidin resistance marker and 100 bp flanking regions of *TcMscS.* Three rotospacer adjacent motifs (PAM) sites within the *TcMscS* gene were identified and guide RNAs (sgRNA) were designed to specifically target the gene. To avoid off target effects, the protospacers were screened against the whole *T.* cruzi genome using ProtoMatch-V 1.0 kindly provided by Sebastian Lourido [113]. The sgRNAs targeting *TcMscS* were amplified with forward primers listed in Table S1 (P7, 8 and 9) and reverse P10

bioRxiv preprint doi: https://doi.org/10.1101/498469; this version posted February 19, 2021. The copyright holder for this preprint (which was not certified by peer review) is the author/funder. All rights reserved. No reuse allowed without permission.

using plasmid pUC_sgRNA as template [98]. The amplicons were cloned into TOPO-Blunt vector and subcloned into sgRNA/Cas9/pTREXn vector. Successful cloning of TcMscS-sgRNAs was confirmed by sequencing. Two donor templates were constructed using the gene encoding blasticidin-S deaminase (Bsd) amplified from tdTomato/pTREX-b [98] and the ultramers indicated in Table S1 (P9-12). The first donor template contained 5' and 3'-UTR regions of *TcMscS* flanking the *Bsd* cassette . The second donor template had the *Bsd gene* flanked by the last 100 bp of coding sequence of *TcMscS* and 100 bp of the 3'-UTR. Plasmid containing a scrambled sgRNA and Cas9 in a pTREXn vector were used as controls. To simplify the labeling the cell line expressing Cas9 and the scrambled sgRNA is labeled Cas9.

Cell transfections

Y-strain epimastigotes were grown for 4 days under standard conditions, collected at 1600 × *g* for 10 minutes, washed once with BAG, and resuspended in 100 µL of Human T Cell Nucleofector Solution (Lonza). 5×10^7 cells were mixed with 5 µg of each sgRNA plasmid with or without 5 µg of DNA donor and electroporated under the U-033 Amaxa Nucleofector protocol. Cells were allowed to recover overnight and appropriate antibiotics for selection (250 µg/mL G-418 and 15 µg/mL of blasticidin) were added.

Genomic screening of transfectants

Clonal populations were obtained by serial dilutions, selected for 3 weeks and a total of 12 clones were screened for proper gene targeting or replacement. Total genomic DNA was extracted from WT, Cas9, TcMscS-KD and TcMscS-KO and analyzed by PCR to evaluate the presence of *TcMscS* (Table S1 P1-2) or the DNA donors (Table S1 P3-4 for blasticidin, P5-6 *TcMscS* downstream). GADPH amplification was used as a housekeeping gene for loading control (Table S1, P15-16). PCR results were confirmed by genomic DNA sequencing.

Strain complementation

The complemented strains C1 and C2 were generated by introducing a copy of TcMscS where the PAM sequence downstream of the sgRNA was mutated by PCR with primers P17 and P18

bioRxiv preprint doi: https://doi.org/10.1101/498469; this version posted February 19, 2021. The copyright holder for this preprint (which was not certified by peer review) is the author/funder. All rights reserved. No reuse allowed without permission.

572 (Table S1). The PAM-mutated ORF of *TcMscS* was amplified (primers P19-P20, Table S1) and
573 subcloned into pTREX-p-myc with HindIII- XhoI restriction sites. The mutation was verified by
574 sequencing and transfected into TcMscS-KO epimastigotes as described above.
575 Complemented strain C3 was obtained by overexpressing a copy of *T. brucei* homolog TbMscS.
576 For that, Tb427.10.9030 sequence was amplified from genomic DNA extracted from WT
577 procyclic forms 427 strain (purchased from BEI Resources) with primers P21-P22 (Table S1),
578 and subcloned into pTREX-p-myc with restriction sites HindIII-XhoI. The complementation
579 plasmid was transfected into TcMscS-KO epimastigotes and the parasites were selected with
580 puromycin (2.5 μg/ml) for 5 weeks. The expression of the myc-tagged proteins was verified by
581 western-blot with monoclonal anti-myc antibodies.
582 *TcMscS expression levels*
583 TcMscS mRNA expression was assessed by RT-qPCR in the three life stages of the parasite as
584 well as in WT, Cas9, TcMscS-KD and TcMscS-KO. Epimastigotes were collected during mid-log
585 phase of growth, washed once with 1x PBS pH 7.4 and homogenized in TRI Reagent®. Total
586 mRNA was extracted following the manufacturer protocol (Sigma-Aldrich, St. Louis, MO)
587 followed by chloroform/ ethanol precipitation cDNA was obtained using SuperScript® III First-
588 Strand Synthesis System (ThermoFisher Scientific, Inc. Waltham, MA) and oligo-$dT_{(20)}$ primers.
589 cDNA was analyzed by qPCR with Power SYBR Green PCR Master Mix (Applied Biosystems)
590 and primers P1-P2 for *TcMscS.* Trypomastigotes were collected by centrifugation from
591 supernatants of infected HEK-293 cells at 5 days post-infection. Amastigotes were collected
592 from by mechanical lysis of infected HEK-293 cells at 3 days post-infections. RNA extraction
593 and cDNA synthesis were performed as indicated for epimastigotes. All qPCR results were
594 normalized against GAPDH as housekeeping gene (Table S1, P15-16) and indicated as ΔΔCq
595 Mean ± SD of at least 3 independent experiments in triplicate.
596

bioRxiv preprint doi: https://doi.org/10.1101/498469; this version posted February 19, 2021. The copyright holder for this preprint (which was not certified by peer review) is the author/funder. All rights reserved. No reuse allowed without permission.

Growth curves

Growth of epimastigotes was measured in TcMscS-KD, TcMscS-KO, WT and Cas9 control parasites starting at a concentration of 1-5 × 10^6 cells/mL in LIT media supplemented as previously described. The number of parasites was determined daily using a Z Series Coulter Counter (Beckman Coulter) The results are expressed as Mean ± SD of 3 independent experiments, in triplicate.

Osmotic stress assays

Epimastigotes at log phase of growth were collected at 1,600 x *g* for 5 min, washed twice in PBS and resuspended in isosmotic buffer (64 mM NaCl, 4 mM KCl, 1.8 mM $CaCl_2$, 0.53 mM $MgCl_2$, 5.5 mM glucose, 150 mM D-mannitol, 5 mM Hepes-Na, pH 7.4, 282 mOsmol/L) at a cell density of 1 x 10^8/ml. Aliquots of 100 µL of parasites were placed in a 96-well plate in isosmotic buffer and relative cell volume changes after osmotic stress were measured by light scattering method [114]. Briefly, pre-treatment readings of parasites in isosmotic buffer were taken for 3 minutes, followed by addition of 200 µL of hyposmotic buffer (64 mM NaCl, 4 mM KCl, 1.8 mM $CaCl_2$, 0.53 mM $MgCl_2$, 5.5 mM glucose, 5 mM HEPES-Na, pH 7.4) was added for a final osmolarity of 115 mOsmol/L. Alternatively, the cells were subjected to hyperosmotic stress with 200 µL of hyperosmotic buffer (64 mM NaCl, 4 mM KCl, 1.8 mM $CaCl_2$, 0.53 mM $MgCl_2$, 5.5 mM glucose, 500 mM D-mannitol, 5 mM HEPES-Na, pH 7.4). The absorbance at 550 nm was measured every 10 seconds for 12 minutes. Readings were normalized against the average of the three minutes of pre-treatment. Normalized absorbance readings were then converted into a percent volume change using the following equation: $[(V_F - V_i)/V_F] \times 100$, where V_F is the absorbance value at the experimental time point and V_i is the initial absorbance value obtained at the same time point under isosmotic conditions.

bioRxiv preprint doi: https://doi.org/10.1101/498469; this version posted February 19, 2021. The copyright holder for this preprint (which was not certified by peer review) is the author/funder. All rights reserved. No reuse allowed without permission.

The maximum volume change was calculated by peak function analysis between 150-250 sec. The final recovery volume was evaluated between 600-700 sec. Results are the Mean ± SE of 6 independent experiments in triplicate for all cell lines.

Live video microscopy under osmotic stress

WT and TcMscS mutant epimastigotes were loosely adhered to poly-L-lysine treated glass bottom coverslips under isosmotic conditions. After adherence, the epimastigotes were subjected to hyposmotic stress under the same conditions described above. Live video microscopy was taken under DIC illumination for 600 seconds in an Olympus© IX83 inverted microscope system.

Intracellular calcium measurements

Calcium measurements were done in WT (n=9) and TcMscS-KO (n=8) epimastigotes collected at four days of growth. Cells were pelleted at 1600g for 10 minutes at room temperature, washed three times with Buffer-A with Glucose (BAG: in mM NaCl 116, KCl 5.4, $MgSO_4$ 0.8, glucose 5, HEPES 50 pH 7.3) and loaded with 5 µM Fura2-AM (Molecular Probes) in BAG for 30 minutes at 30℃, washed twice and resuspended in BAG at a concentration of $5x10^8$ cells/ml. Aliquots of $5x10^7$ cells were taken for each measurement with excitation at 340/380 nm and emission at 525 nm. Calibration was done by permeabilizing cells in BAG plus 1 mM EGTA and then adding increasing concentrations of $CaCl_2$. The concentration of free calcium available was calculated using MaxChelator software (http://maxchelator.stanford.edu/) and the Kd was calculated according to the manufacturer protocol. Experimental recordings were allowed to stabilize at baseline before addition of 1.8 mM $CaCl_2$ or 10 □M of Bay K8644. Recordings were done on a Hitachi F7000 spectrofluorometer with excitation wavelength 340/380 nm and emission 510 nm.

Statistical analysis

bioRxiv preprint doi: https://doi.org/10.1101/498469; this version posted February 19, 2021. The copyright holder for this preprint (which was not certified by peer review) is the author/funder. All rights reserved. No reuse allowed without permission.

All the experiments were performed at least 3 times unless indicated otherwise, with intra-experiment replicates. The results are presented as Mean ± SD or SE as indicated in the figure legend. Statistical significance was evaluated by one way ANOVA with ad-hoc Bonferroni post-test or Student t- test as indicated in the figures.

Acknowledgments

Dr. Roberto Docampo for his guidance and manuscript revisions, Stephen Vella and Dr. Myriam Hortua-Triana for assistance with super resolution imaging. Dr. Nikolas Nikolaidis kindly provided antibodies against actin.

This work was funded by the National Institute of Health NIAID grant R15AI122153 and American Heart Association grant 16GRNT30280014 to VJ, and scholarship from Cal State Fullerton MARC U*STAR Program grant 2T34GM008612-23 to JF.

bioRxiv preprint doi: https://doi.org/10.1101/498469; this version posted February 19, 2021. The copyright holder for this preprint (which was not certified by peer review) is the author/funder. All rights reserved. No reuse allowed without permission.

Figure legends

Figure 1. Sequence alignment and predictions of TcMscS structure by homology to EcMscS. A. Partial protein sequence alignment of four MscS-type channels from *T. cruzi T. cruzi* Esmeraldo-like (TcCLB.504171.40) and non-Esmeraldo-like (TcCLB.509795.40) haplotypes of the CL Brener reference strain, *T. brucei* (Tb427.10.9030) and *L. major* (LmjF.36.5770), with two bacterial MscS channels from *E. coli* (WP_000389819) and *H. pilory* (WP_000343449.1). The position of the transmembrane domains TM1, TM2 and TM3 are underlined, the position of the putative gate residues are indicated by red arrows, conserved residues forming the hinges of TM3 are indicated with asterisks. The full alignment can be found in supplemental Figure S1. **B**. Arrangements of transmembrane helices of EcMscS (PDB ID 2OAU) and in the proposed homology model of TcMscS. The position of the putative gate and secondary constriction residues for TcMscS (F64 and L97) are indicated**. C.** Full homology TcMscS model in the closed and open states. N-terminal domain 1 (red), TM 2 (gold) and TM 3 (green) are followed by the cytoplasmic cage (cyan) and the C-terminal bundle (blue). The gate residues are indicated in pink and yellow.

Figure 2. Electrophysiological properties of TcMscS. A. Single-channel currents at positive and negative pipette voltages **B.** Current-to-voltage relationships measured in symmetric (200 mM/200 mM KCl, black symbols, n=11) and asymmetric conditions (425mM/200 mM KCl, red symbols, n=4). The theoretical reversal potentials for Cl^- and K^+ (grey arrows) and the experimental reversal potential measured for TcMscS (red arrow) are indicated. **C.** Unitary conductace of TcMscS recorded with 100 mM Ca gluconate, 20 mM $CaCl_2$ in the pipette and 200 mM KCl in the bath at +30 mV in the pipette. **D.** The trace recorded from the same patch after perfusion of the bath with 100 mM Ca gluconate. In the latter configuration (shown on the right), Ca^{2+} is the dominant permeable ion. **E.** Examples of traces recorded with identical 1-s linear ramps on three separate patches bearing 11, 2 and 3 active channels at +30 mV or -30 mV pipette potential. **F.** Multiple ramp responses of TcMscS populations were

bioRxiv preprint doi: https://doi.org/10.1101/498469; this version posted February 19, 2021. The copyright holder for this preprint (which was not certified by peer review) is the author/funder. All rights reserved. No reuse allowed without permission.

normalized to the current at saturating pressure and converted to dose-response curves. The aggregated TcMscS curve (blue symbols, n=11) is compared with EcMscS dose-response curves (black symbols, n=54). The inset in panel **D** shows the same dose-response curves plotted as log (Po/Pc) and fitted with the Boltzmann equation. The shallower slope of the TcMscS dose-response curve indicates a smaller lateral expansion of the protein complex.

Figure 3. Localization and expression of TcMscS in *T. cruzi*. Immunolocalization of TcMscS (red) with specific polyclonal antibodies in epimastigotes **(A)**, trypomastigotes **(B)** and intracellular amastigotes **(C).** The right panels correspond to images of the same life stages obtained by super-resolution microscopy. Cellular structures are indicated as CV (contractile vacuole), K (kinetoplast) and N (nucleus). DNA was DAPI stained. Bar sizes: A = 5 µm; B and C = 5 µm. **D.** Expression of TcMscS in different life stages of the parasite, quantified by RT-qPCR. Trypomastigotes (Tryp) and amastigotes (Amast) were obtained from HEK-293 cells. Epimastigotes were analyzed at 4 days (Epis Exp) and 10 days of growth (Epis Stat). The values are indicated as ΔΔCq respect to the expression in trypomastigotes and normalized against GAPDH as housekeeping gene. The values are Mean ± SEM of 3 independent experiments in triplicate (* *p = 0.006, # p = 0.009*). **E.** Western blot analysis of TcMscS in trypomastigotes (T), amastigotes (A) and epimastigotes (E). Purified recombinant protein (R) was used as positive control. The whole cell lysates were probed with polyclonal antibodies against TcMscS and monoclonal anti-tubulin was used as loading control.

Figure 4. TcMscS colocalization with organelle markers. A. Immunofluorescence analysis of TcMscS (red) localization in epimastigotes overexpressing TcVAMP-GFP (green). **B.** Labeling of TcMscS (red) in WT Y strain epimastigotes partially colocalizes with anti-actin antibodies (green). **C.** Localization of TcMscS (red) and tubulin (green) in Y strain epimastigotes. No significant colocalization was observed. **D.** Immunolocalization of TcMscS (red) and membrane marker SSP-1 (green) in Y strain tissue-derived trypomastigotes. **E.** Co-localization of TcMscS

bioRxiv preprint doi: https://doi.org/10.1101/498469; this version posted February 19, 2021. The copyright holder for this preprint (which was not certified by peer review) is the author/funder. All rights reserved. No reuse allowed without permission.

(red) and membrane marker SSP-4 (green) in extracellular amastigotes obtained by host cell lysis. Nuclei and kinetoplasts were DAPI stained. Arrows indicate the position of the contractile vacuole. Bar size: 5 µm.

Figure 5. Phenotypic characterization of TcMscS KO. A. Schematic representation of *TcMcS* gene targeting by CRISPR/Cas9. A double strand DNA cut was induced at position +185 and repaired by homologous recombination with construct containing the *Bsd gene*. The primers used for screening are listed in Table S1. **B.** gDNA screening of TcMscS KO epimastigotes by PCR. Negative controls (C) without DNA are in lane 1 for all reactions. The ORF for *TcMscS* was amplified in WT and Cas9 controls but absent in TcMscS KO parasites. The correct insertion of the blasticidin cassette (BSD) was verified by amplification with primers annealing in ORF and the 3'UTR. GAPDH was used as a housekeeping gene for loading control. **C.** Growth curve of epimastigotes WT (black line), Cas9 (red line), TcMscS KD (blue line) and TcMscS KO (green line). All the experiments were started at $1x10^6$/ ml cells and counted daily. The values are Mean ± SEM of 3 independent experiments in triplicate (*, ** $p<0.01$). **D.** RT-qPCR quantifying the expression of TcMscS in epimastigotes control (Cas9) vs TcMscS-KO. The values are indicated as ΔΔCq respect to the expression in WT epimastigotes and normalized against GAPDH as housekeeping gene. All the samples were collected from parasites at 4 days of growth. The values are Mean ± SEM of 3 independent experiments in triplicate (# p = *0.0001*). **E.** Immunofluorescence analysis of TcMscS (red) in epimastigotes Y strain (WT), TcMscS-KO. Nuclei and kinetoplasts were DAPI stained. The position of the contractile vacuole is indicated with yellow arrows. Bar size= 2 µm.

Figure 6. Osmotic stress responses in TcMscS mutants. A. Regulatory volume decreases in epimastigotes. Cells suspended in isosmotic buffer recorded for 120 sec and diluted with to a final osmolarity of 115 mOsm/L under constant ionic conditions. Relative changes in cell volume were monitored by determining absorbance at 550 nm over time, in WT (black), Cas9 (red),

bioRxiv preprint doi: https://doi.org/10.1101/498469; this version posted February 19, 2021. The copyright holder for this preprint (which was not certified by peer review) is the author/funder. All rights reserved. No reuse allowed without permission.

TcMscS-KD (blue) and TcMscS-KO (green). The absorbance values were normalized by the initial volume under isosmotic conditions and expressed as percentage of volume change. **B.** Analysis of the maximum volume change under hypoosmotic conditions. The peak area was calculated between 150-250 sec for all the experiments. **C.** Final volume recovery calculated between 600-700 sec. **D.** Volume decrease in epimastigotes after hyperosmotic shock. After 3 min under isosmotic conditions, cells were placed under hyperosmotic stress at 650 mOsm/L. Volume changes were monitored and calculated as explained in **A.** Peak analysis **(E)** and final volumes were calculated at the same times that in **B** and **C.** The values for A-F are mean ± SEM of 6 independent experiments in triplicate ($p< 0.001$). Statistical analysis details are listed in Table S2 and S3. **G.** Representative immunofluorescence images of WT and TcMscS-KO epimastigotes at 2 min post hypo-osmotic stress. TcMscS (red) was detected with specific polyclonal antibodies against the channel. Nuclei and kinetoplasts were DAPI stained. Yellow arrows indicate the presence of cells with abnormal morphology, observed in the TcMscS-KO strain. Bar size= 2 µm.

Figure 7. Intracellular calcium measurements. **A** and **C** are representative traces of intracellular calcium level in WT (black line) or TcMscS-KO (green line) epimastigotes loaded with Fura 2-AM at baseline or after the addition of 1.8 mM $CaCl_2$ and 10 µM of Bay K8644. **B** and **D** show the quantification of baseline Ca^{2+} concentration in the first 75 s and on the first 100 s after addition of the stimuli for WT (black) and TcMscS-KO (green) for multiple experiments. The values are Mean ± SE of n=7 independent experiments (*$p<0.01$, ***$p<0.001$, ****$p< 0.0001$).

Figure 8. Infectivity defects in TcMscS mutants. A. Representative immunofluorescence images showing the localization of TcMscS in metacyclic trypomastigotes labeled with anti-TcMscS antibodies (red). The position of the contractile vacuole is indicated by yellow arrows. Nuclei and kinetoplasts were DAPI stained. Bar size= 2 µm. **B.** Percentage of metacyclic forms

bioRxiv preprint doi: https://doi.org/10.1101/498469; this version posted February 19, 2021. The copyright holder for this preprint (which was not certified by peer review) is the author/funder. All rights reserved. No reuse allowed without permission.

obtained *in vitro* from WT and TcMscS-KO parasites incubated for 72 h in TAU 3AAG media. Values are mean ± SEM of 5 independent experiments. **C.** Quantification of intracellular amastigotes at 48 h post infection. HEK 293 cells were infected at a MOI of 25:1 with trypomastigotes WT (black), Cas9 (red), TcMscS-KD (blue) or TcMscS-KO (green). TcMscS mutants show a significant decrease in intracellular amastigotes. Values are mean ± SEM of 5 independent experiments in triplicate. **D.** Quantification of extracellular trypomastigotes released from infected HEK293 cells after 4 days of infection. Cells were infected at a MOI of 25:1 with WT (black), Cas9 (red) or TcMscS-KO (green) trypomastigotes and extracellular parasites were collected daily for counting. Values are mean ± SEM of 4 independent experiments. **E.** Representative images of HEK293 cells infected with Cas9 (Cas9), TcMscS-KD or TcMscS-KO parasites. TcMscS was detected with specific antibodies (red), Cas9 was labeled with anti-GFP, nuclei and kinetoplasts were DAPI stained. Bar size= 10 µm. (**p<0.01, ****p< 0.0001).

bioRxiv preprint doi: https://doi.org/10.1101/498469; this version posted February 19, 2021. The copyright holder for this preprint (which was not certified by peer review) is the author/funder. All rights reserved. No reuse allowed without permission.

References

1. Cox CD, Bavi N, Martinac B. Bacterial Mechanosensors. Annual review of physiology. 2017. Epub 2017/12/02. doi: 10.1146/annurev-physiol-021317-121351. PubMed PMID: 29195054.
2. Arnadottir J, Chalfie M. Eukaryotic mechanosensitive channels. Annual review of biophysics. 2010;39:111-37. Epub 2010/03/03. doi: 10.1146/annurev.biophys.37.032807.125836. PubMed PMID: 20192782.
3. Peyronnet R, Tran D, Girault T, Frachisse JM. Mechanosensitive channels: feeling tension in a world under pressure. Frontiers in plant science. 2014;5:558. Epub 2014/11/07. doi: 10.3389/fpls.2014.00558. PubMed PMID: 25374575; PubMed Central PMCID: PMCPMC4204436.
4. Martinac B, Buechner M, Delcour AH, Adler J, Kung C. Pressure-sensitive ion channel in Escherichia coli. Proceedings of the National Academy of Sciences of the United States of America. 1987;84(8):2297-301. PubMed PMID: 2436228; PubMed Central PMCID: PMCPMC304637.
5. Sukharev SI, Martinac B, Arshavsky VY, Kung C. Two types of mechanosensitive channels in the Escherichia coli cell envelope: solubilization and functional reconstitution. Biophysical journal. 1993;65(1):177-83. doi: 10.1016/S0006-3495(93)81044-0. PubMed PMID: 7690260; PubMed Central PMCID: PMCPMC1225713.
6. Martinac B. Bacterial mechanosensitive channels as a paradigm for mechanosensory transduction. Cellular physiology and biochemistry : international journal of experimental cellular physiology, biochemistry, and pharmacology. 2011;28(6):1051-60. Epub 2011/12/20. doi: 10.1159/000335842. PubMed PMID: 22178995.
7. Cox CD, Nomura T, Ziegler CS, Campbell AK, Wann KT, Martinac B. Selectivity mechanism of the mechanosensitive channel MscS revealed by probing channel subconducting states. Nature communications. 2013;4:2137. Epub 2013/07/12. doi: 10.1038/ncomms3137. PubMed PMID: 23842527.
8. Maksaev G, Haswell ES. Recent characterizations of MscS and its homologs provide insight into the basis of ion selectivity in mechanosensitive channels. Channels (Austin, Tex). 2013;7(3):215-20. Epub 2013/04/18. doi: 10.4161/chan.24505. PubMed PMID: 23590902; PubMed Central PMCID: PMCPMC3710349.
9. Li J, Hou B, Tumova S, Muraki K, Bruns A, Ludlow MJ, et al. Piezo1 integration of vascular architecture with physiological force. Nature. 2014;515:279. doi: 10.1038/nature13701 https://www.nature.com/articles/nature13701#supplementary-information.
10. Miura S, Sato K, Kato-Negishi M, Teshima T, Takeuchi S. Fluid shear triggers microvilli formation via mechanosensitive activation of TRPV6. Nature communications. 2015;6:8871. Epub 2015/11/14. doi: 10.1038/ncomms9871. PubMed PMID: 26563429; PubMed Central PMCID: PMCPMC4660203.
11. Corrigan MA, Johnson GP, Stavenschi E, Riffault M, Labour MN, Hoey DA. TRPV4-mediates oscillatory fluid shear mechanotransduction in mesenchymal stem cells in part via the primary cilium. Sci Rep. 2018;8(1):3824. Epub 2018/03/02. doi: 10.1038/s41598-018-22174-3. PubMed PMID: 29491434; PubMed Central PMCID: PMCPMC5830574.
12. Engler AJ, Sen S, Sweeney HL, Discher DE. Matrix elasticity directs stem cell lineage specification. Cell. 2006;126(4):677-89. Epub 2006/08/23. doi: 10.1016/j.cell.2006.06.044. PubMed PMID: 16923388.
13. He L, Ahmad M, Perrimon N. Mechanosensitive channels and their functions in stem cell differentiation. Experimental Cell Research. 2019;374(2):259-65. doi: https://doi.org/10.1016/j.yexcr.2018.11.016.
14. Koser DE, Thompson AJ, Foster SK, Dwivedy A, Pillai EK, Sheridan GK, et al. Mechanosensing is critical for axon growth in the developing brain. Nat Neurosci.

bioRxiv preprint doi: https://doi.org/10.1101/498469; this version posted February 19, 2021. The copyright holder for this preprint (which was not certified by peer review) is the author/funder. All rights reserved. No reuse allowed without permission.

2016;19(12):1592-8. Epub 2016/11/01. doi: 10.1038/nn.4394. PubMed PMID: 27643431; PubMed Central PMCID: PMCPMC5531257.

15. Irvine KD, Shraiman BI. Mechanical control of growth: ideas, facts and challenges. Development. 2017;144(23):4238-48. doi: 10.1242/dev.151902.

16. Shraiman BI. Mechanical feedback as a possible regulator of tissue growth. Proceedings of the National Academy of Sciences of the United States of America. 2005;102(9):3318-23. Epub 2005/02/25. doi: 10.1073/pnas.0404782102. PubMed PMID: 15728365; PubMed Central PMCID: PMCPMC552900.

17. Barnes JM, Przybyla L, Weaver VM. Tissue mechanics regulate brain development, homeostasis and disease. J Cell Sci. 2017;130(1):71-82. Epub 2017/01/04. doi: 10.1242/jcs.191742. PubMed PMID: 28043968; PubMed Central PMCID: PMCPMC5394781.

18. Broders-Bondon F, Nguyen Ho-Bouldoires TH, Fernandez-Sanchez ME, Farge E. Mechanotransduction in tumor progression: The dark side of the force. J Cell Biol. 2018;217(5):1571-87. Epub 2018/02/23. doi: 10.1083/jcb.201701039. PubMed PMID: 29467174; PubMed Central PMCID: PMCPMC5940296.

19. Siryaporn A, Kuchma SL, O'Toole GA, Gitai Z. Surface attachment induces Pseudomonas aeruginosa virulence. Proceedings of the National Academy of Sciences of the United States of America. 2014;111(47):16860-5. Epub 2014/11/12. doi: 10.1073/pnas.1415712111. PubMed PMID: 25385640; PubMed Central PMCID: PMCPMC4250119.

20. O'Loughlin CT, Miller LC, Siryaporn A, Drescher K, Semmelhack MF, Bassler BL. A quorum-sensing inhibitor blocks Pseudomonas aeruginosa virulence and biofilm formation. Proceedings of the National Academy of Sciences of the United States of America. 2013;110(44):17981-6. Epub 2013/10/22. doi: 10.1073/pnas.1316981110. PubMed PMID: 24143808; PubMed Central PMCID: PMCPMC3816427.

21. Thomen P, Robert J, Monmeyran A, Bitbol AF, Douarche C, Henry N. Bacterial biofilm under flow: First a physical struggle to stay, then a matter of breathing. PloS one. 2017;12(4):e0175197. Epub 2017/04/14. doi: 10.1371/journal.pone.0175197. PubMed PMID: 28403171; PubMed Central PMCID: PMCPMC5389662.

22. Prindle A, Liu J, Asally M, Ly S, Garcia-Ojalvo J, Suel GM. Ion channels enable electrical communication in bacterial communities. Nature. 2015;527(7576):59-63. Epub 2015/10/28. doi: 10.1038/nature15709. PubMed PMID: 26503040; PubMed Central PMCID: PMCPMC4890463.

23. Harker KS, Jivan E, McWhorter FY, Liu WF, Lodoen MB. Shear forces enhance Toxoplasma gondii tachyzoite motility on vascular endothelium. MBio. 2014;5(2):e01111-13. doi: 10.1128/mBio.01111-13. PubMed PMID: 24692639; PubMed Central PMCID: PMCPMC3977363.

24. Sumpio BJ, Chitragari G, Moriguchi T, Shalaby S, Pappas-Brown V, Khan AM, et al. African Trypanosome-Induced Blood-Brain Barrier Dysfunction under Shear Stress May Not Require ERK Activation. Int J Angiol. 2015;24(1):41-6. Epub 2016/04/08. doi: 10.1055/s-0034-1370890. PubMed PMID: 27053915; PubMed Central PMCID: PMCPMC4813428.

25. Laperchia C, Palomba M, Seke Etet PF, Rodgers J, Bradley B, Montague P, et al. Trypanosoma brucei Invasion and T-Cell Infiltration of the Brain Parenchyma in Experimental Sleeping Sickness: Timing and Correlation with Functional Changes. PLoS Negl Trop Dis. 2016;10(12):e0005242. Epub 2016/12/22. doi: 10.1371/journal.pntd.0005242. PubMed PMID: 28002454; PubMed Central PMCID: PMCPMC5217973.

26. Coates BM, Sullivan DP, Makanji MY, Du NY, Olson CL, Muller WA, et al. Endothelial transmigration by Trypanosoma cruzi. PloS one. 2013;8(12):e81187. Epub 2013/12/07. doi: 10.1371/journal.pone.0081187. PubMed PMID: 24312535; PubMed Central PMCID: PMCPMC3846899.

27. Barragan A, Brossier F, Sibley LD. Transepithelial migration of Toxoplasma gondii involves an interaction of intercellular adhesion molecule 1 (ICAM-1) with the parasite adhesin

bioRxiv preprint doi: https://doi.org/10.1101/498469; this version posted February 19, 2021. The copyright holder for this preprint (which was not certified by peer review) is the author/funder. All rights reserved. No reuse allowed without permission.

MIC2. Cellular microbiology. 2005;7(4):561-8. Epub 2005/03/12. doi: 10.1111/j.1462-5822.2005.00486.x. PubMed PMID: 15760456.

28. Barragan A, Sibley LD. Transepithelial migration of Toxoplasma gondii is linked to parasite motility and virulence. J Exp Med. 2002;195(12):1625-33. Epub 2002/06/19. PubMed PMID: 12070289; PubMed Central PMCID: PMCPMC2193562.

29. Capewell P, Cren-Travaille C, Marchesi F, Johnston P, Clucas C, Benson RA, et al. The skin is a significant but overlooked anatomical reservoir for vector-borne African trypanosomes. Elife. 2016;5. Epub 2016/09/23. doi: 10.7554/eLife.17716. PubMed PMID: 27653219; PubMed Central PMCID: PMCPMC5065312.

30. Trindade S, Rijo-Ferreira F, Carvalho T, Pinto-Neves D, Guegan F, Aresta-Branco F, et al. Trypanosoma brucei Parasites Occupy and Functionally Adapt to the Adipose Tissue in Mice. Cell Host Microbe. 2016;19(6):837-48. Epub 2016/05/31. doi: 10.1016/j.chom.2016.05.002. PubMed PMID: 27237364; PubMed Central PMCID: PMCPMC4906371.

31. Mattos EC, Canuto G, Manchola NC, Magalhaes RDM, Crozier TWM, Lamont DJ, et al. Reprogramming of Trypanosoma cruzi metabolism triggered by parasite interaction with the host cell extracellular matrix. PLoS Negl Trop Dis. 2019;13(2):e0007103. Epub 2019/02/07. doi: 10.1371/journal.pntd.0007103. PubMed PMID: 30726203.

32. Perez-Molina JA, Molina I. Chagas disease. Lancet. 2018;391(10115):82-94. Epub 2017/07/05. doi: 10.1016/S0140-6736(17)31612-4. PubMed PMID: 28673423.

33. Requena-Mendez A, Aldasoro E, de Lazzari E, Sicuri E, Brown M, Moore DA, et al. Prevalence of Chagas disease in Latin-American migrants living in Europe: a systematic review and meta-analysis. PLoS Negl Trop Dis. 2015;9(2):e0003540. Epub 2015/02/14. doi: 10.1371/journal.pntd.0003540. PubMed PMID: 25680190; PubMed Central PMCID: PMCPMC4332678.

34. Bern C, Montgomery SP. An estimate of the burden of Chagas disease in the United States. Clin Infect Dis. 2009;49(5):e52-4. Epub 2009/07/31. doi: 10.1086/605091. PubMed PMID: 19640226.

35. Jimenez V. Dealing with environmental challenges: mechanisms of adaptation in Trypanosoma cruzi. Res Microbiol. 2014;165(3):155-65. doi: 10.1016/j.resmic.2014.01.006. PubMed PMID: 24508488; PubMed Central PMCID: PMCPMC3997592.

36. Cowman AF, Healer J, Marapana D, Marsh K. Malaria: Biology and Disease. Cell. 2016;167(3):610-24. doi: 10.1016/j.cell.2016.07.055.

37. Silvester E, McWilliam KR, Matthews KR. The Cytological Events and Molecular Control of Life Cycle Development of Trypanosoma brucei in the Mammalian Bloodstream. Pathogens. 2017;6(3). Epub 2017/06/29. doi: 10.3390/pathogens6030029. PubMed PMID: 28657594; PubMed Central PMCID: PMCPMC5617986.

38. Kollien AH, Schaub GA. Development of Trypanosoma cruzi after starvation and feeding of the vector - a review. The Tokai journal of experimental and clinical medicine. 1998;23(6):335-40. Epub 2000/01/06. PubMed PMID: 10622631.

39. Ward AI, Lewis MD, Khan AA, McCann CJ, Francisco AF, Jayawardhana S, et al. In Vivo Analysis of Trypanosoma cruzi Persistence Foci at Single-Cell Resolution. mBio. 2020;11(4). Epub 2020/08/06. doi: 10.1128/mBio.01242-20. PubMed PMID: 32753495; PubMed Central PMCID: PMCPMC7407085.

40. Blair CA, Pruitt BL. Mechanobiology Assays with Applications in Cardiomyocyte Biology and Cardiotoxicity. Adv Healthc Mater. 2020;9(8):e1901656. Epub 2020/04/10. doi: 10.1002/adhm.201901656. PubMed PMID: 32270928; PubMed Central PMCID: PMCPMC7480481.

41. Rohloff P, Montalvetti A, Docampo R. Acidocalcisomes and the contractile vacuole complex are involved in osmoregulation in Trypanosoma cruzi. The Journal of biological

bioRxiv preprint doi: https://doi.org/10.1101/498469; this version posted February 19, 2021. The copyright holder for this preprint (which was not certified by peer review) is the author/funder. All rights reserved. No reuse allowed without permission.

chemistry. 2004;279(50):52270-81. Epub 2004/10/07. doi: 10.1074/jbc.M410372200. PubMed PMID: 15466463.

42. Furuya T, Kashuba C, Docampo R, Moreno SN. A novel phosphatidylinositol-phospholipase C of Trypanosoma cruzi that is lipid modified and activated during trypomastigote to amastigote differentiation. The Journal of biological chemistry. 2000;275(9):6428-38. PubMed PMID: 10692446.

43. Moreno SN, Silva J, Vercesi AE, Docampo R. Cytosolic-free calcium elevation in Trypanosoma cruzi is required for cell invasion. J Exp Med. 1994;180(4):1535-40. PubMed PMID: 7931085; PubMed Central PMCID: PMCPMC2191711.

44. Tardieux I, Nathanson MH, Andrews NW. Role in host cell invasion of Trypanosoma cruzi-induced cytosolic-free Ca2+ transients. J Exp Med. 1994;179(3):1017-22. PubMed PMID: 8113670; PubMed Central PMCID: PMCPMC2191425.

45. Lander N, Chiurillo MA, Docampo R. Signaling pathways involved in environmental sensing in Trypanosoma cruzi. Mol Microbiol. 2020. Epub 2020/10/10. doi: 10.1111/mmi.14621. PubMed PMID: 33034088.

46. Chiurillo MA, Lander N, Bertolini MS, Storey M, Vercesi AE, Docampo R. Different Roles of Mitochondrial Calcium Uniporter Complex Subunits in Growth and Infectivity of Trypanosoma cruzi. MBio. 2017;8(3). Epub 2017/05/11. doi: 10.1128/mBio.00574-17. PubMed PMID: 28487431; PubMed Central PMCID: PMCPMC5424207.

47. Rohloff P, Docampo R. A contractile vacuole complex is involved in osmoregulation in Trypanosoma cruzi. Exp Parasitol. 2008;118(1):17-24. Epub 2007/06/19. doi: 10.1016/j.exppara.2007.04.013. PubMed PMID: 17574552; PubMed Central PMCID: PMCPMC2243178.

48. Docampo R, Jimenez V, Lander N, Li ZH, Niyogi S. New insights into roles of acidocalcisomes and contractile vacuole complex in osmoregulation in protists. Int Rev Cell Mol Biol. 2013;305:69-113. Epub 2013/07/31. doi: 10.1016/b978-0-12-407695-2.00002-0. PubMed PMID: 23890380; PubMed Central PMCID: PMCPMC3818246.

49. Allen RD, Naitoh Y. Osmoregulation and contractile vacuoles of protozoa. Int Rev Cytol. 2002;215:351-94. Epub 2002/04/16. PubMed PMID: 11952235.

50. Palmer CP, Zhou XL, Lin J, Loukin SH, Kung C, Saimi Y. A TRP homolog in Saccharomyces cerevisiae forms an intracellular Ca(2+)-permeable channel in the yeast vacuolar membrane. Proceedings of the National Academy of Sciences of the United States of America. 2001;98(14):7801-5. doi: 10.1073/pnas.141036198. PubMed PMID: 11427713; PubMed Central PMCID: PMCPMC35422.

51. Lee CP, Maksaev G, Jensen GS, Murcha MW, Wilson ME, Fricker M, et al. MSL1 is a mechanosensitive ion channel that dissipates mitochondrial membrane potential and maintains redox homeostasis in mitochondria during abiotic stress. The Plant journal : for cell and molecular biology. 2016;88(5):809-25. Epub 2016/11/04. doi: 10.1111/tpj.13301. PubMed PMID: 27505616; PubMed Central PMCID: PMCPMC5195915.

52. Peyronnet R, Haswell ES, Barbier-Brygoo H, Frachisse JM. AtMSL9 and AtMSL10: Sensors of plasma membrane tension in Arabidopsis roots. Plant signaling & behavior. 2008;3(9):726-9. Epub 2009/08/26. PubMed PMID: 19704841; PubMed Central PMCID: PMCPMC2634572.

53. Haswell ES, Meyerowitz EM. MscS-like proteins control plastid size and shape in Arabidopsis thaliana. Curr Biol. 2006;16(1):1-11. doi: 10.1016/j.cub.2005.11.044. PubMed PMID: 16401419.

54. Sukharev SI, Blount P, Martinac B, Blattner FR, Kung C. A large-conductance mechanosensitive channel in E. coli encoded by mscL alone. Nature. 1994;368(6468):265-8. doi: 10.1038/368265a0. PubMed PMID: 7511799.

55. Levina N, Tötemeyer S, Stokes NR, Louis P, Jones MA, Booth IR. Protection of Escherichia coli cells against extreme turgor by activation of MscS and MscL

bioRxiv preprint doi: https://doi.org/10.1101/498469; this version posted February 19, 2021. The copyright holder for this preprint (which was not certified by peer review) is the author/funder. All rights reserved. No reuse allowed without permission.

mechanosensitive channels: identification of genes required for MscS activity. The EMBO Journal. 1999;18(7):1730-7. doi: 10.1093/emboj/18.7.1730.

56. Kloda A, Martinac B. Molecular identification of a mechanosensitive channel in archaea. Biophysical journal. 2001;80(1):229-40. doi: 10.1016/S0006-3495(01)76009-2. PubMed PMID: 11159397; PubMed Central PMCID: PMCPMC1301228.

57. Prole DL, Taylor CW. Identification and analysis of putative homologues of mechanosensitive channels in pathogenic protozoa. PloS one. 2013;8(6):e66068. Epub 2013/06/21. doi: 10.1371/journal.pone.0066068. PubMed PMID: 23785469; PubMed Central PMCID: PMCPMC3681921.

58. Bass RB, Strop P, Barclay M, Rees DC. Crystal structure of Escherichia coli MscS, a voltage-modulated and mechanosensitive channel. Science (New York, NY). 2002;298(5598):1582-7. Epub 2002/11/26. doi: 10.1126/science.1077945. PubMed PMID: 12446901.

59. Anishkin A, Gendel V, Sharifi NA, Chiang CS, Shirinian L, Guy HR, et al. On the conformation of the COOH-terminal domain of the large mechanosensitive channel MscL. The Journal of general physiology. 2003;121(3):227-44. Epub 2003/02/26. doi: 10.1085/jgp.20028768. PubMed PMID: 12601086; PubMed Central PMCID: PMCPMC2217331.

60. Sukharev S. Purification of the small mechanosensitive channel of Escherichia coli (MscS): the subunit structure, conduction, and gating characteristics in liposomes. Biophysical journal. 2002;83(1):290-8. doi: 10.1016/S0006-3495(02)75169-2. PubMed PMID: 12080120; PubMed Central PMCID: PMCPMC1302147.

61. Belyy V, Kamaraju K, Akitake B, Anishkin A, Sukharev S. Adaptive behavior of bacterial mechanosensitive channels is coupled to membrane mechanics. The Journal of general physiology. 2010;135(6):641-52. Epub 2010/06/02. doi: 10.1085/jgp.200910371. PubMed PMID: 20513760; PubMed Central PMCID: PMCPMC2888061.

62. Chiang CS, Anishkin A, Sukharev S. Gating of the large mechanosensitive channel in situ: estimation of the spatial scale of the transition from channel population responses. Biophysical journal. 2004;86(5):2846-61. Epub 2004/04/28. doi: 10.1016/S0006-3495(04)74337-4. PubMed PMID: 15111402; PubMed Central PMCID: PMCPMC1304154.

63. Anishkin A, Akitake B, Sukharev S. Characterization of the resting MscS: modeling and analysis of the closed bacterial mechanosensitive channel of small conductance. Biophysical journal. 2008;94(4):1252-66. Epub 2007/11/06. doi: 10.1529/biophysj.107.110171. PubMed PMID: 17981908; PubMed Central PMCID: PMCPMC2212706.

64. Ulrich PN, Jimenez V, Park M, Martins VP, Atwood J, 3rd, Moles K, et al. Identification of contractile vacuole proteins in Trypanosoma cruzi. PloS one. 2011;6(3):e18013. Epub 2011/03/26. doi: 10.1371/journal.pone.0018013. PubMed PMID: 21437209; PubMed Central PMCID: PMCPMC3060929.

65. Niyogi S, Jimenez V, Girard-Dias W, de Souza W, Miranda K, Docampo R. Rab32 is essential for maintaining functional acidocalcisomes, and for growth and infectivity of Trypanosoma cruzi. J Cell Sci. 2015;128(12):2363-73. doi: 10.1242/jcs.169466. PubMed PMID: 25964650; PubMed Central PMCID: PMCPMC4487017.

66. Aistleitner K, Heinz C, Hormann A, Heinz E, Montanaro J, Schulz F, et al. Identification and characterization of a novel porin family highlights a major difference in the outer membrane of chlamydial symbionts and pathogens. PloS one. 2013;8(1):e55010. Epub 2013/02/06. doi: 10.1371/journal.pone.0055010. PubMed PMID: 23383036; PubMed Central PMCID: PMCPMC3561449.

67. Ghosh R, Steiert M, Hardmeyer A, Wang YF, Rosenbusch JP. Overexpression of outer membrane porins in E. coli using pBluescript-derived vectors. Gene Expr. 1998;7(3):149-61. Epub 1998/12/05. PubMed PMID: 9840808; PubMed Central PMCID: PMCPMC6151949.

68. Li ZH, Alvarez VE, De Gaudenzi JG, Sant'Anna C, Frasch AC, Cazzulo JJ, et al. Hyperosmotic stress induces aquaporin-dependent cell shrinkage, polyphosphate synthesis,

bioRxiv preprint doi: https://doi.org/10.1101/498469; this version posted February 19, 2021. The copyright holder for this preprint (which was not certified by peer review) is the author/funder. All rights reserved. No reuse allowed without permission.

amino acid accumulation, and global gene expression changes in Trypanosoma cruzi. The Journal of biological chemistry. 2011;286(51):43959-71. Epub 2011/11/01. doi: 10.1074/jbc.M111.311530. PubMed PMID: 22039054; PubMed Central PMCID: PMCPMC3243512.

69. Rodriguez-Duran J, Pinto-Martinez A, Castillo C, Benaim G. Identification and electrophysiological properties of a sphingosine-dependent plasma membrane Ca(2+) channel in Trypanosoma cruzi. FEBS J. 2019;286(19):3909-25. Epub 2019/06/05. doi: 10.1111/febs.14947. PubMed PMID: 31162791.

70. Contreras VT, Salles JM, Thomas N, Morel CM, Goldenberg S. In vitro differentiation of Trypanosoma cruzi under chemically defined conditions. Molecular and biochemical parasitology. 1985;16(3):315-27. Epub 1985/09/01. PubMed PMID: 3903496.

71. Malcolm HR, Maurer JA. The mechanosensitive channel of small conductance (MscS) superfamily: not just mechanosensitive channels anymore. Chembiochem : a European journal of chemical biology. 2012;13(14):2037-43. Epub 2012/08/24. doi: 10.1002/cbic.201200410. PubMed PMID: 22915507.

72. Kumamoto CA. Molecular mechanisms of mechanosensing and their roles in fungal contact sensing. Nat Rev Microbiol. 2008;6(9):667-73. doi: 10.1038/nrmicro1960. PubMed PMID: 18679170; PubMed Central PMCID: PMCPMC2760928.

73. Nakayama Y, Yoshimura K, Iida H. Organellar mechanosensitive channels in fission yeast regulate the hypo-osmotic shock response. Nature communications. 2012;3:1020. doi: 10.1038/ncomms2014. PubMed PMID: 22910366.

74. Nakayama Y, Hirata A, Iida H. Mechanosensitive channels Msy1 and Msy2 are required for maintaining organelle integrity upon hypoosmotic shock in Schizosaccharomyces pombe. FEMS Yeast Res. 2014;14(6):992-4. Epub 2014/07/22. doi: 10.1111/1567-1364.12181. PubMed PMID: 25041276.

75. Tominaga T, Naitoh Y. COMPARISON BETWEEN THERMORECEPTOR AND MECHANORECEPTOR CURRENTS IN PARAMECIUM CAUDATUM. J Exp Biol. 1994;189(1):117-31. PubMed PMID: 9317455.

76. Yoshimura K. Mechanosensitive channels in the cell body of Chlamydomonas. J Membr Biol. 1998;166(2):149-55. PubMed PMID: 9841739.

77. Nakayama Y, Fujiu K, Sokabe M, Yoshimura K. Molecular and electrophysiological characterization of a mechanosensitive channel expressed in the chloroplasts of Chlamydomonas. Proceedings of the National Academy of Sciences of the United States of America. 2007;104(14):5883-8. doi: 10.1073/pnas.0609996104. PubMed PMID: 17389370; PubMed Central PMCID: PMCPMC1851586.

78. Maksaev G, Haswell ES. MscS-Like10 is a stretch-activated ion channel from Arabidopsis thaliana with a preference for anions. Proceedings of the National Academy of Sciences of the United States of America. 2012;109(46):19015-20. doi: 10.1073/pnas.1213931109. PubMed PMID: 23112188; PubMed Central PMCID: PMCPMC3503204.

79. Wilson ME, Jensen GS, Haswell ES. Two mechanosensitive channel homologs influence division ring placement in Arabidopsis chloroplasts. The Plant cell. 2011;23(8):2939-49. doi: 10.1105/tpc.111.088112. PubMed PMID: 21810996; PubMed Central PMCID: PMCPMC3180802.

80. Kloda A, Martinac B. Common evolutionary origins of mechanosensitive ion channels in Archaea, Bacteria and cell-walled Eukarya. Archaea. 2002;1(1):35-44. PubMed PMID: 15803657; PubMed Central PMCID: PMCPMC2685541.

81. Nakayama Y, Komazawa K, Bavi N, Hashimoto KI, Kawasaki H, Martinac B. Evolutionary specialization of MscCG, an MscS-like mechanosensitive channel, in amino acid transport in Corynebacterium glutamicum. Sci Rep. 2018;8(1):12893. Epub 2018/08/29. doi:

bioRxiv preprint doi: https://doi.org/10.1101/498469; this version posted February 19, 2021. The copyright holder for this preprint (which was not certified by peer review) is the author/funder. All rights reserved. No reuse allowed without permission.

10.1038/s41598-018-31219-6. PubMed PMID: 30150671; PubMed Central PMCID: PMCPMC6110860.

82. Becker M, Borngen K, Nomura T, Battle AR, Marin K, Martinac B, et al. Glutamate efflux mediated by Corynebacterium glutamicum MscCG, Escherichia coli MscS, and their derivatives. Biochimica et biophysica acta. 2013;1828(4):1230-40. Epub 2013/01/15. doi: 10.1016/j.bbamem.2013.01.001. PubMed PMID: 23313454.

83. Nakayama Y, Iida H. Organellar mechanosensitive channels involved in hypo-osmoregulation in fission yeast. Cell calcium. 2014;56(6):467-71. Epub 2014/12/03. doi: 10.1016/j.ceca.2014.10.001. PubMed PMID: 25454595.

84. Wilson ME, Basu MR, Bhaskara GB, Verslues PE, Haswell ES. Plastid osmotic stress activates cellular stress responses in Arabidopsis. Plant physiology. 2014;165(1):119-28. doi: 10.1104/pp.114.236620. PubMed PMID: 24676856; PubMed Central PMCID: PMCPMC4012573.

85. Wilson M, Haswell E. A role for mechanosensitive channels in chloroplast and bacterial fission. Plant signaling & behavior. 2012;7(2):157-60. Epub 2012/02/07. doi: 10.4161/psb.18735. PubMed PMID: 22307046; PubMed Central PMCID: PMCPMC3405697.

86. Cox CD, Nakayama Y, Nomura T, Martinac B. The evolutionary 'tinkering' of MscS-like channels: generation of structural and functional diversity. Pflugers Archiv : European journal of physiology. 2015;467(1):3-13. Epub 2014/05/14. doi: 10.1007/s00424-014-1522-2. PubMed PMID: 24819593.

87. Rohloff P, Rodrigues CO, Docampo R. Regulatory volume decrease in Trypanosoma cruzi involves amino acid efflux and changes in intracellular calcium. Molecular and biochemical parasitology. 2003;126(2):219-30. Epub 2003/03/05. PubMed PMID: 12615321.

88. Blount P, Sukharev SI, Moe PC, Schroeder MJ, Guy HR, Kung C. Membrane topology and multimeric structure of a mechanosensitive channel protein of Escherichia coli. EMBO J. 1996;15(18):4798-805. Epub 1996/09/16. PubMed PMID: 8890153; PubMed Central PMCID: PMCPMC452216.

89. Fujiu K, Nakayama Y, Iida H, Sokabe M, Yoshimura K. Mechanoreception in motile flagella of Chlamydomonas. Nat Cell Biol. 2011;13(5):630-2. doi: 10.1038/ncb2214. PubMed PMID: 21478860.

90. Plattner H. Contractile vacuole complex--its expanding protein inventory. Int Rev Cell Mol Biol. 2013;306:371-416. doi: 10.1016/B978-0-12-407694-5.00009-2. PubMed PMID: 24016530.

91. Denis V, Cyert MS. Internal Ca(2+) release in yeast is triggered by hypertonic shock and mediated by a TRP channel homologue. J Cell Biol. 2002;156(1):29-34. doi: 10.1083/jcb.200111004. PubMed PMID: 11781332; PubMed Central PMCID: PMCPMC2173594.

92. Tominaga T, Allen R, y. Electrophysiology of the in situ contractile vacuole complex of Paramecium reveals its membrane dynamics and electrogenic site during osmoregulatory activity. J Exp Biol. 1998;201(3):451-60. PubMed PMID: 9427677.

93. Tani T, Allen RD, Naitoh Y. Periodic tension development in the membrane of the in vitro contractile vacuole of Paramecium multimicronucleatum: modification by bisection, fusion and suction. J Exp Biol. 2000;203(Pt 2):239-51. Epub 1999/12/23. PubMed PMID: 10607534.

94. de Melo TG, Meirelles Mde N, Pereira MC. Trypanosoma cruzi alters adherens junctions in cardiomyocytes. Microbes Infect. 2008;10(12-13):1405-10. Epub 2008/09/10. doi: 10.1016/j.micinf.2008.07.044. PubMed PMID: 18778790.

95. Melo TG, Almeida DS, Meirelles MN, Pereira MC. Disarray of sarcomeric alpha-actinin in cardiomyocytes infected by Trypanosoma cruzi. Parasitology. 2006;133(Pt 2):171-8. Epub 2006/05/03. doi: 10.1017/S0031182006000011. PubMed PMID: 16650336.

bioRxiv preprint doi: https://doi.org/10.1101/498469; this version posted February 19, 2021. The copyright holder for this preprint (which was not certified by peer review) is the author/funder. All rights reserved. No reuse allowed without permission.

96. Melo TG, Almeida DS, de Meirelles Mde N, Pereira MC. Trypanosoma cruzi infection disrupts vinculin costameres in cardiomyocytes. Eur J Cell Biol. 2004;83(10):531-40. Epub 2005/02/01. doi: 10.1078/0171-9335-00419. PubMed PMID: 15679099.
97. Mott A, Lenormand G, Costales J, Fredberg JJ, Burleigh BA. Modulation of host cell mechanics by Trypanosoma cruzi. J Cell Physiol. 2009;218(2):315-22. Epub 2008/10/15. doi: 10.1002/jcp.21606. PubMed PMID: 18853412; PubMed Central PMCID: PMCPMC2592505.
98. Lander N, Li ZH, Niyogi S, Docampo R. CRISPR/Cas9-Induced Disruption of Paraflagellar Rod Protein 1 and 2 Genes in Trypanosoma cruzi Reveals Their Role in Flagellar Attachment. MBio. 2015;6(4). doi: 10.1128/mBio.01012-15. PubMed PMID: 26199333.
99. Li P, Bian X, Liu C, Wang S, Guo M, Tao Y, et al. STIM1 and TRPV4 regulate fluid flow-induced calcium oscillation at early and late stages of osteoclast differentiation. Cell calcium. 2018;71:45-52. doi: https://doi.org/10.1016/j.ceca.2017.12.001.
100. Lu J, Fan Y, Gong X, Zhou X, Yi C, Zhang Y, et al. The Lineage Specification of Mesenchymal Stem Cells Is Directed by the Rate of Fluid Shear Stress. Journal of Cellular Physiology. 2016;231(8):1752-60. doi: doi:10.1002/jcp.25278.
101. Shimogawa MM, Ray SS, Kisalu N, Zhang Y, Geng Q, Ozcan A, et al. Parasite motility is critical for virulence of African trypanosomes. Sci Rep. 2018;8(1):9122. Epub 2018/06/16. doi: 10.1038/s41598-018-27228-0. PubMed PMID: 29904094; PubMed Central PMCID: PMCPMC6002391.
102. Edwards BFL, Wheeler RJ, Barker AR, Moreira-Leite FF, Gull K, Sunter JD. Direction of flagellum beat propagation is controlled by proximal/distal outer dynein arm asymmetry. Proceedings of the National Academy of Sciences of the United States of America. 2018;115(31):E7341-e50. Epub 2018/07/22. doi: 10.1073/pnas.1805827115. PubMed PMID: 30030284; PubMed Central PMCID: PMCPMC6077732.
103. Collingridge P, Brownlee C, Wheeler Glen L. Compartmentalized Calcium Signaling in Cilia Regulates Intraflagellar Transport. Current Biology. 2013;23(22):2311-8. doi: 10.1016/j.cub.2013.09.059.
104. Nauli SM, Kawanabe Y, Kaminski JJ, Pearce WJ, Ingber DE, Zhou J. Endothelial cilia are fluid shear sensors that regulate calcium signaling and nitric oxide production through polycystin-1. Circulation. 2008;117(9):1161-71. Epub 2008/02/21. doi: 10.1161/CIRCULATIONAHA.107.710111. PubMed PMID: 18285569; PubMed Central PMCID: PMCPMC3071982.
105. Wu L, Gao X, Brown RC, Heller S, O'Neil RG. Dual role of the TRPV4 channel as a sensor of flow and osmolality in renal epithelial cells. Am J Physiol Renal Physiol. 2007;293(5):F1699-713. Epub 2007/08/19. doi: 10.1152/ajprenal.00462.2006. PubMed PMID: 17699550.
106. Schmid A, Salathe M. Ciliary beat co-ordination by calcium. Biology of the cell. 2011;103(4):159-69. doi: doi:10.1042/BC20100120.
107. Shimogawa MM, Saada EA, Vashisht AA, Barshop WD, Wohlschlegel JA, Hill KL. Cell Surface Proteomics Provides Insight into Stage-Specific Remodeling of the Host-Parasite Interface in Trypanosoma brucei. Molecular & cellular proteomics : MCP. 2015;14(7):1977-88. Epub 2015/05/13. doi: 10.1074/mcp.M114.045146. PubMed PMID: 25963835; PubMed Central PMCID: PMCPMC4587323.
108. Docampo R, Huang G. Calcium signaling in trypanosomatid parasites. Cell calcium. 2014. doi: 10.1016/j.ceca.2014.10.015. PubMed PMID: 25468729.
109. Cruz-Bustos T, Moreno SNJ, Docampo R. Detection of Weakly Expressed Trypanosoma cruzi Membrane Proteins Using High-Performance Probes. J Eukaryot Microbiol. 2018;65(5):722-8. Epub 2018/03/16. doi: 10.1111/jeu.12517. PubMed PMID: 29542839; PubMed Central PMCID: PMCPMC6120783.
110. Edwards MD, Black S, Rasmussen T, Rasmussen A, Stokes NR, Stephen TL, et al. Characterization of three novel mechanosensitive channel activities in Escherichia coli.

bioRxiv preprint doi: https://doi.org/10.1101/498469; this version posted February 19, 2021. The copyright holder for this preprint (which was not certified by peer review) is the author/funder. All rights reserved. No reuse allowed without permission.

Channels (Austin, Tex). 2012;6(4):272-81. Epub 2012/08/10. doi: 10.4161/chan.20998. PubMed PMID: 22874652; PubMed Central PMCID: PMCPMC3508906.

111. Delcour AH, Martinac B, Adler J, Kung C. Modified reconstitution method used in patch-clamp studies of Escherichia coli ion channels. Biophysical journal. 1989;56(3):631-6. doi: 10.1016/S0006-3495(89)82710-9. PubMed PMID: 2477074; PubMed Central PMCID: PMCPMC1280516.

112. Bone GJ, Steinert M. Isotopes incorporated in the nucleic acids of Trypanosoma mega. Nature. 1956;178(4528):308-9. Epub 1956/08/11. PubMed PMID: 13358724.

113. Sidik SM, Hackett CG, Tran F, Westwood NJ, Lourido S. Efficient genome engineering of Toxoplasma gondii using CRISPR/Cas9. PloS one. 2014;9(6):e100450. Epub 2014/06/28. doi: 10.1371/journal.pone.0100450. PubMed PMID: 24971596; PubMed Central PMCID: PMCPMC4074098.

114. Jimenez V, Docampo R. Molecular and electrophysiological characterization of a novel cation channel of Trypanosoma cruzi. PLoS Pathog. 2012;8(6):e1002750. Epub 2012/06/12. doi: 10.1371/journal.ppat.1002750. PubMed PMID: 22685407; PubMed Central PMCID: PMCPMC3369953.

bioRxiv preprint doi: https://doi.org/10.1101/498469; this version posted February 19, 2021. The copyright holder for this preprint (which was not certified by peer review) is the author/funder. All rights reserved. No reuse allowed without permission.

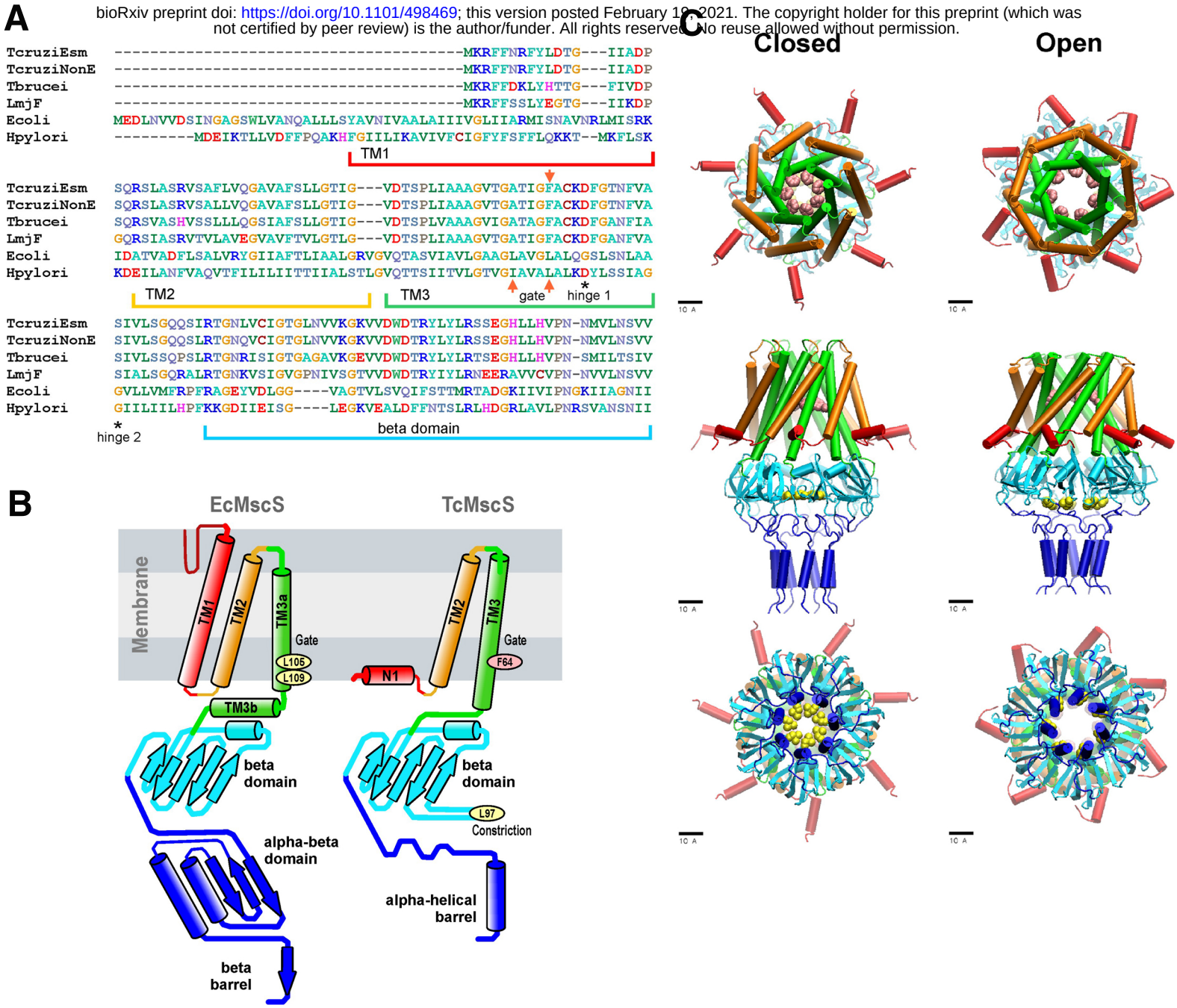

Fig. 1

bioRxiv preprint doi: https://doi.org/10.1101/498469; this version posted February 19, 2021. The copyright holder for this preprint (which was not certified by peer review) is the author/funder. All rights reserved. No reuse allowed without permission.

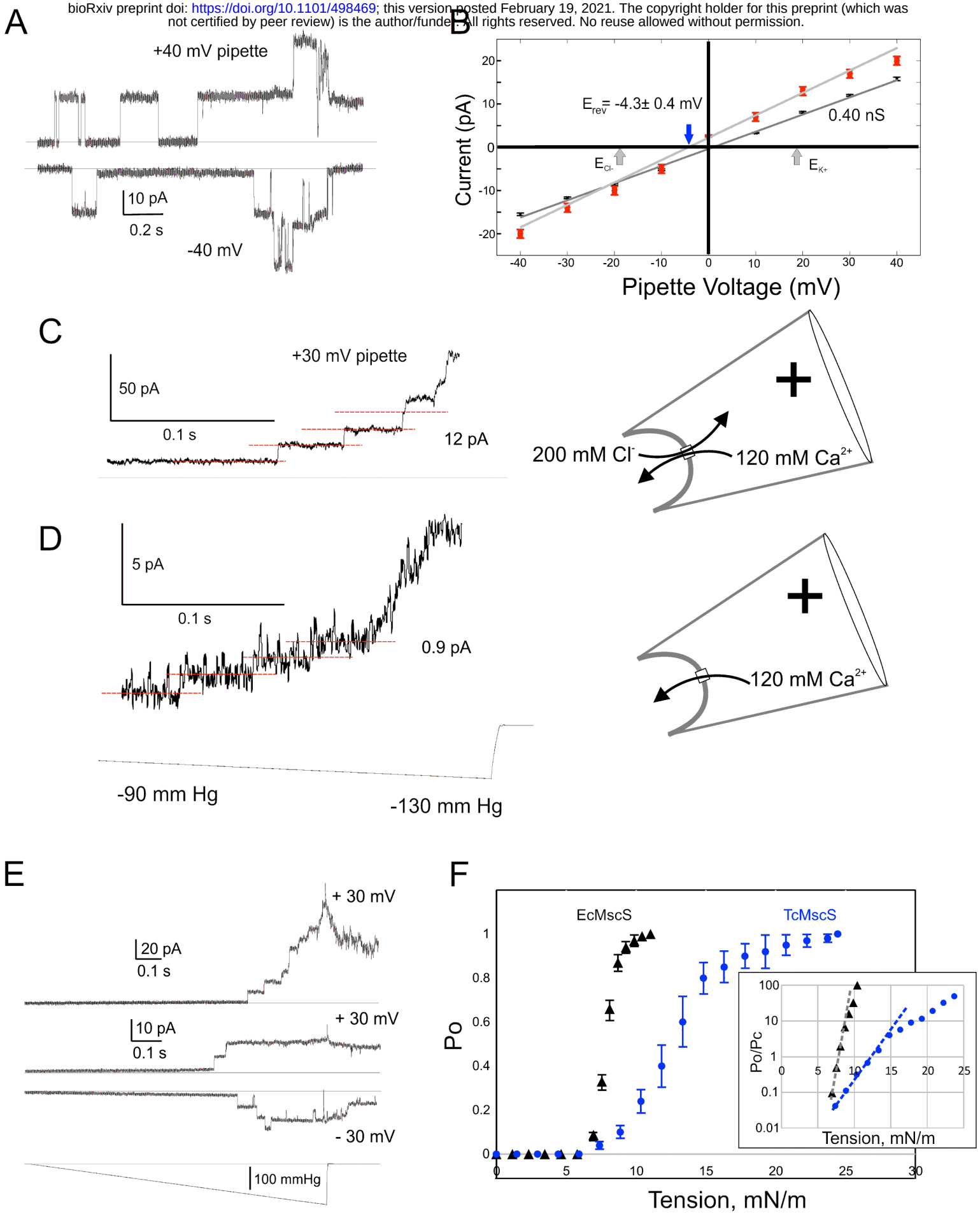

Fig. 2

bioRxiv preprint doi: https://doi.org/10.1101/498469; this version posted February 19, 2021. The copyright holder for this preprint (which was not certified by peer review) is the author/funder. All rights reserved. No reuse allowed without permission.

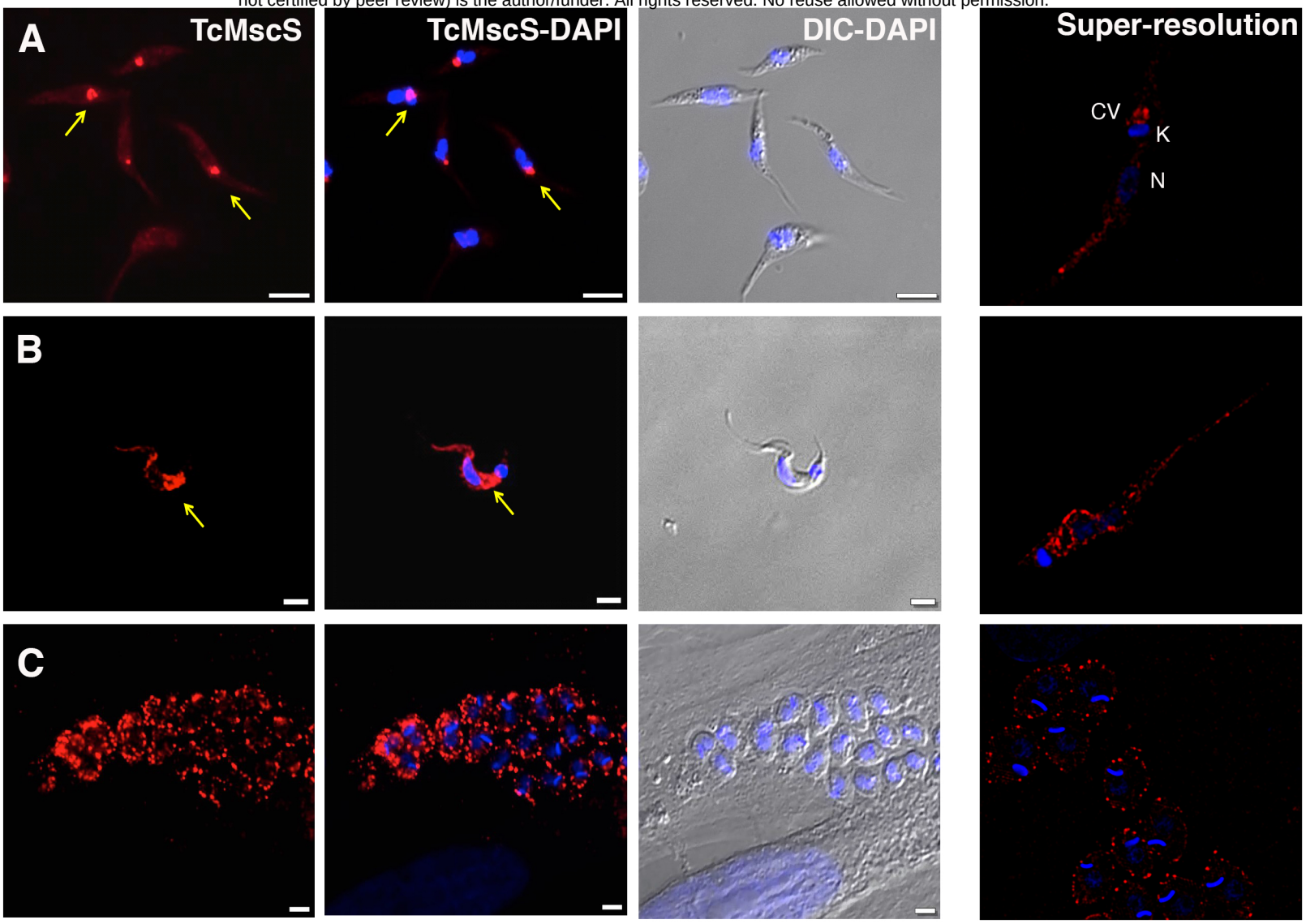

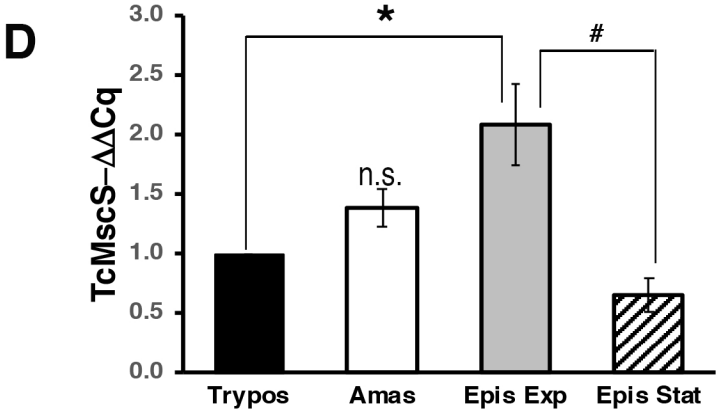

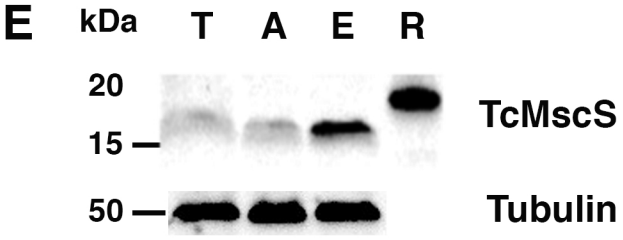

Fig. 3

bioRxiv preprint doi: https://doi.org/10.1101/498469; this version posted February 19, 2021. The copyright holder for this preprint (which was not certified by peer review) is the author/funder. All rights reserved. No reuse allowed without permission.

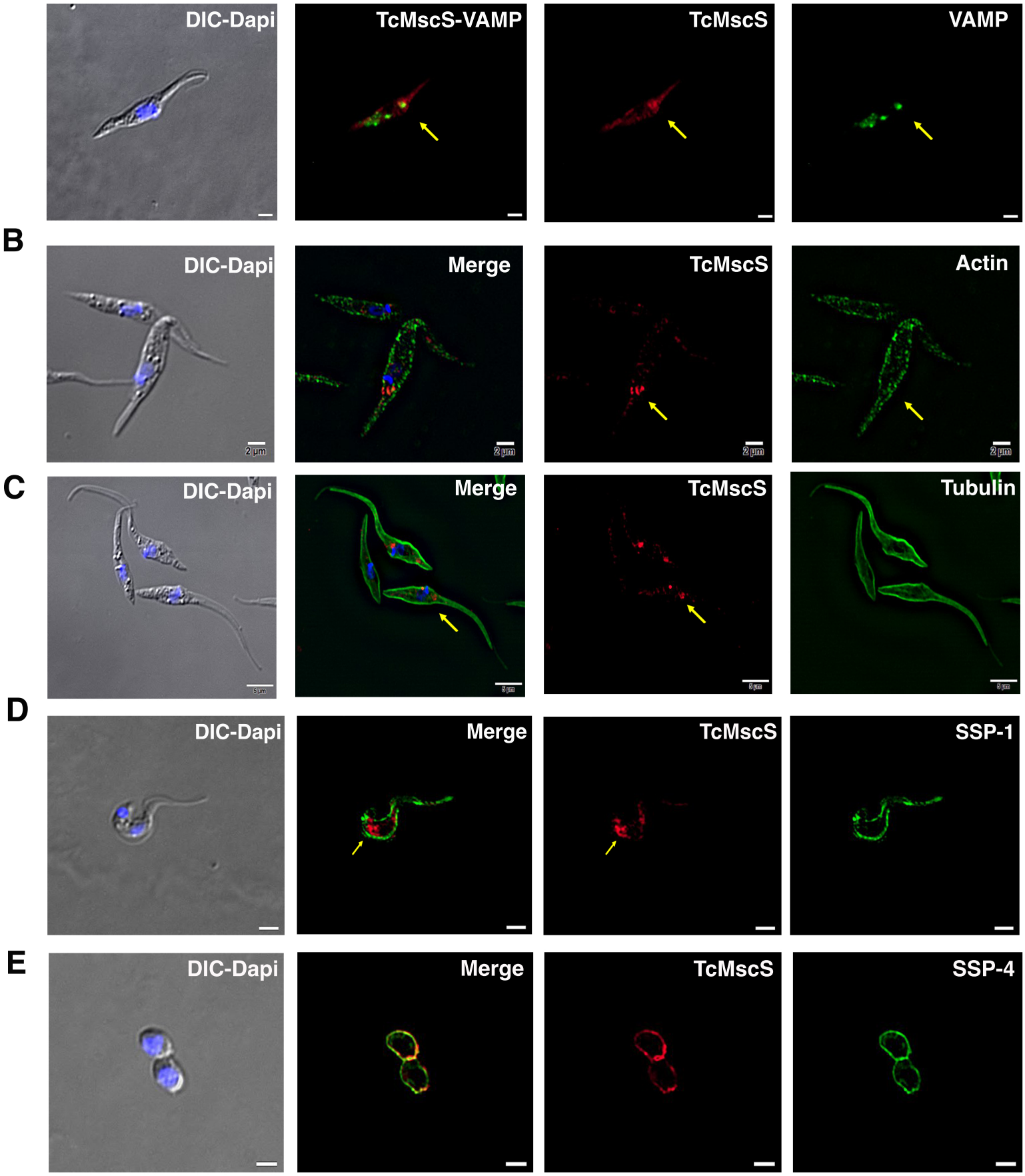

Fig. 4

bioRxiv preprint doi: https://doi.org/10.1101/498469; this version posted February 19, 2021. The copyright holder for this preprint (which was not certified by peer review) is the author/funder. All rights reserved. No reuse allowed without permission.

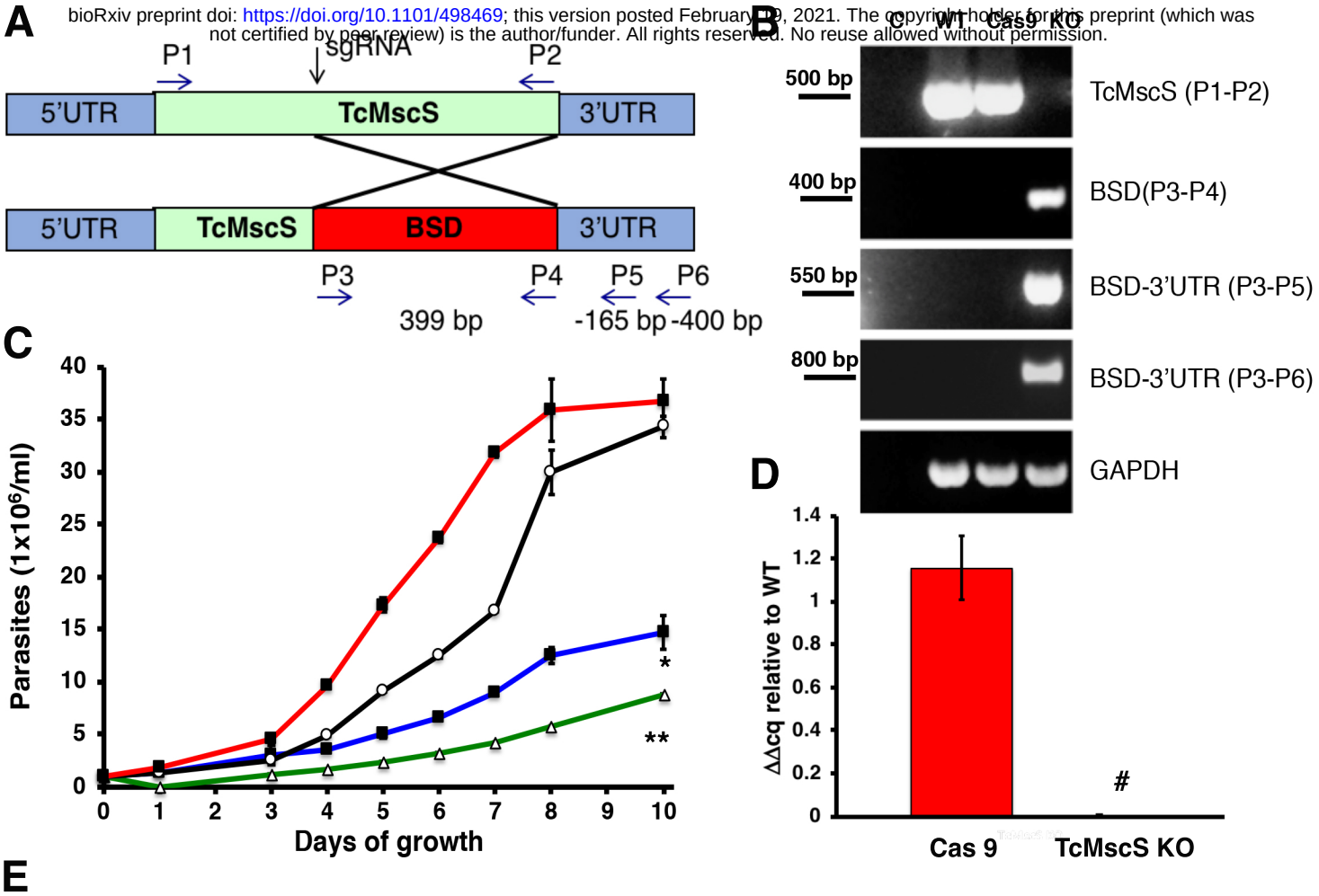

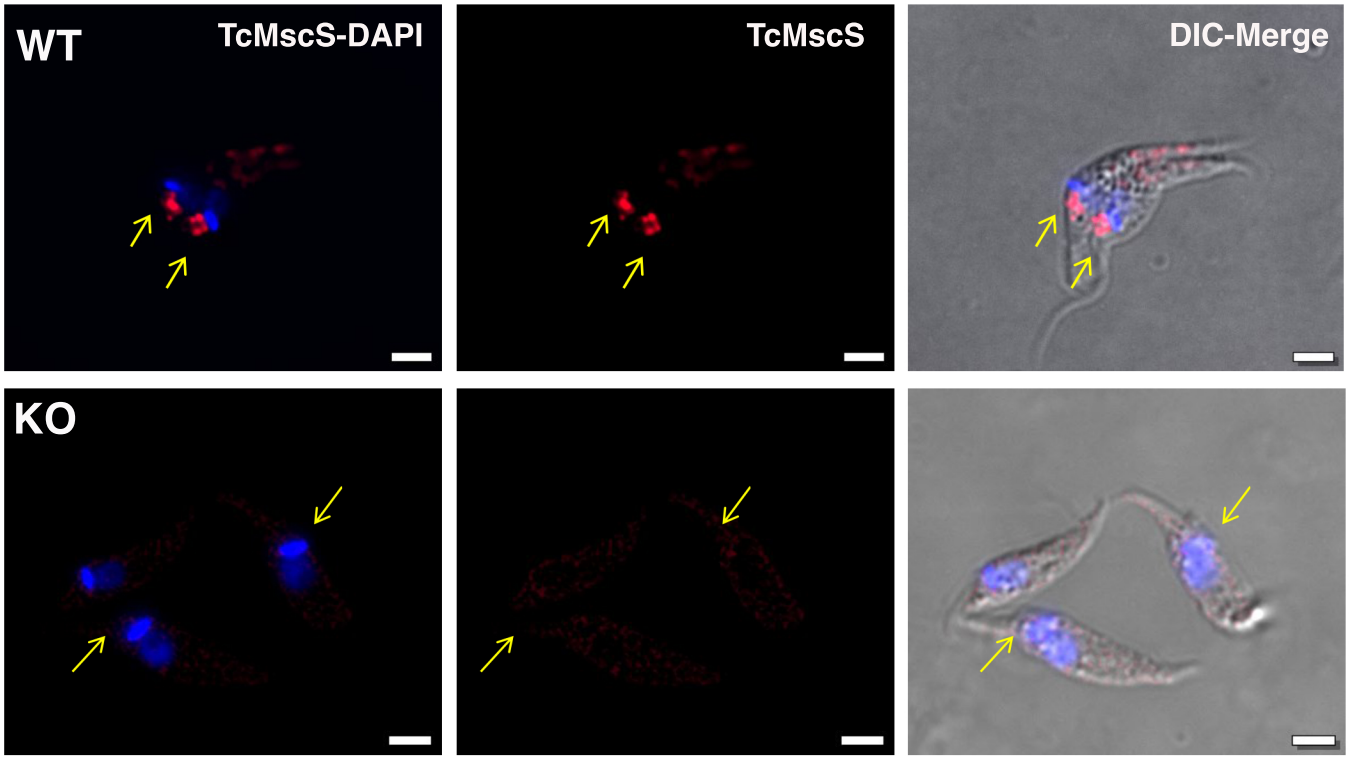

Fig. 5

bioRxiv preprint doi: https://doi.org/10.1101/498469; the version posted February 19, 2021. The copyright holder for this preprint (which was not certified by peer review) is the author/funder. All rights reserved. No reuse allowed without permission.

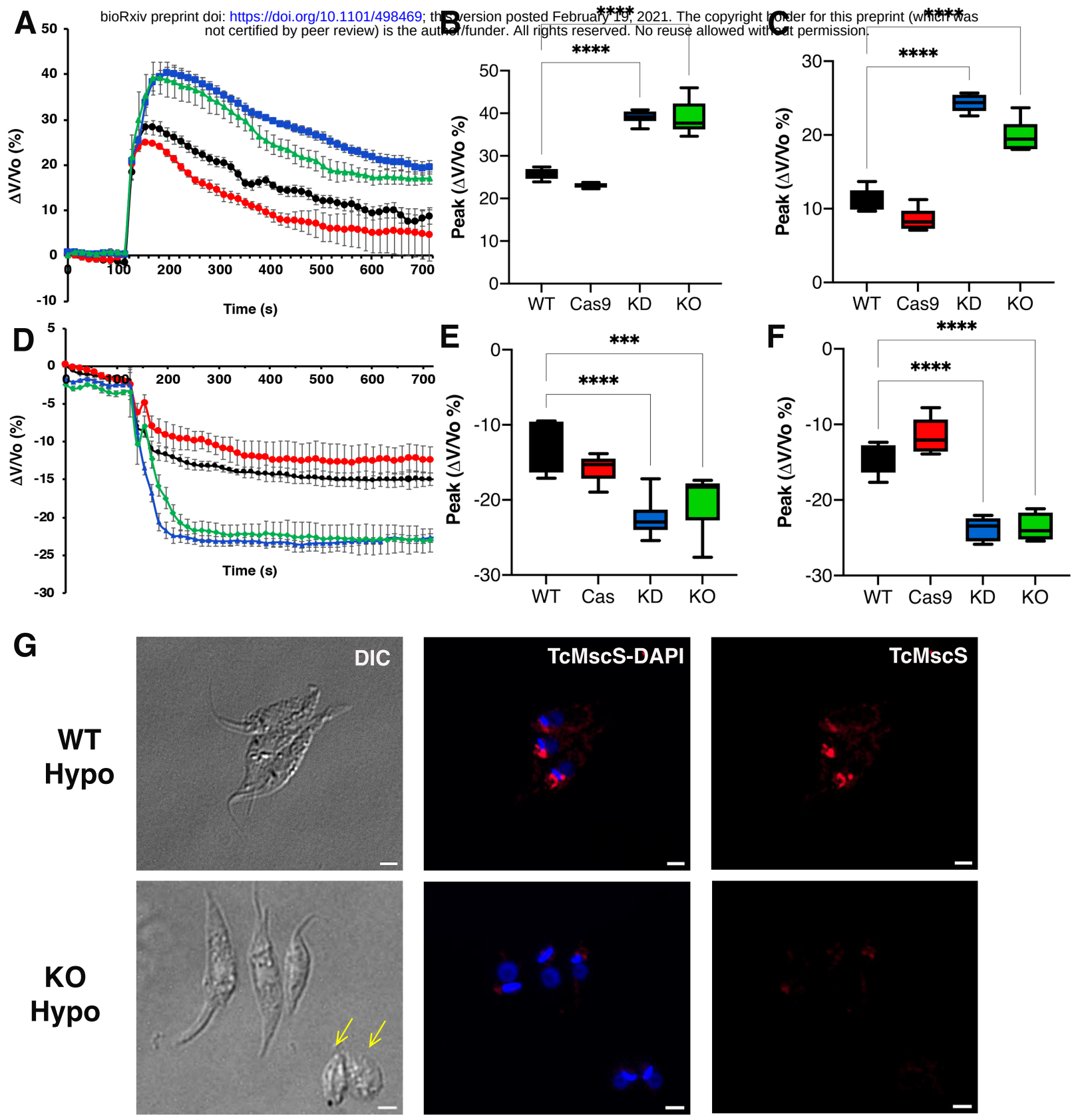

Fig. 6

bioRxiv preprint doi: https://doi.org/10.1101/498469; this version posted February 19, 2021. The copyright holder for this preprint (which was not certified by peer review) is the author/funder. All rights reserved. No reuse allowed without permission.

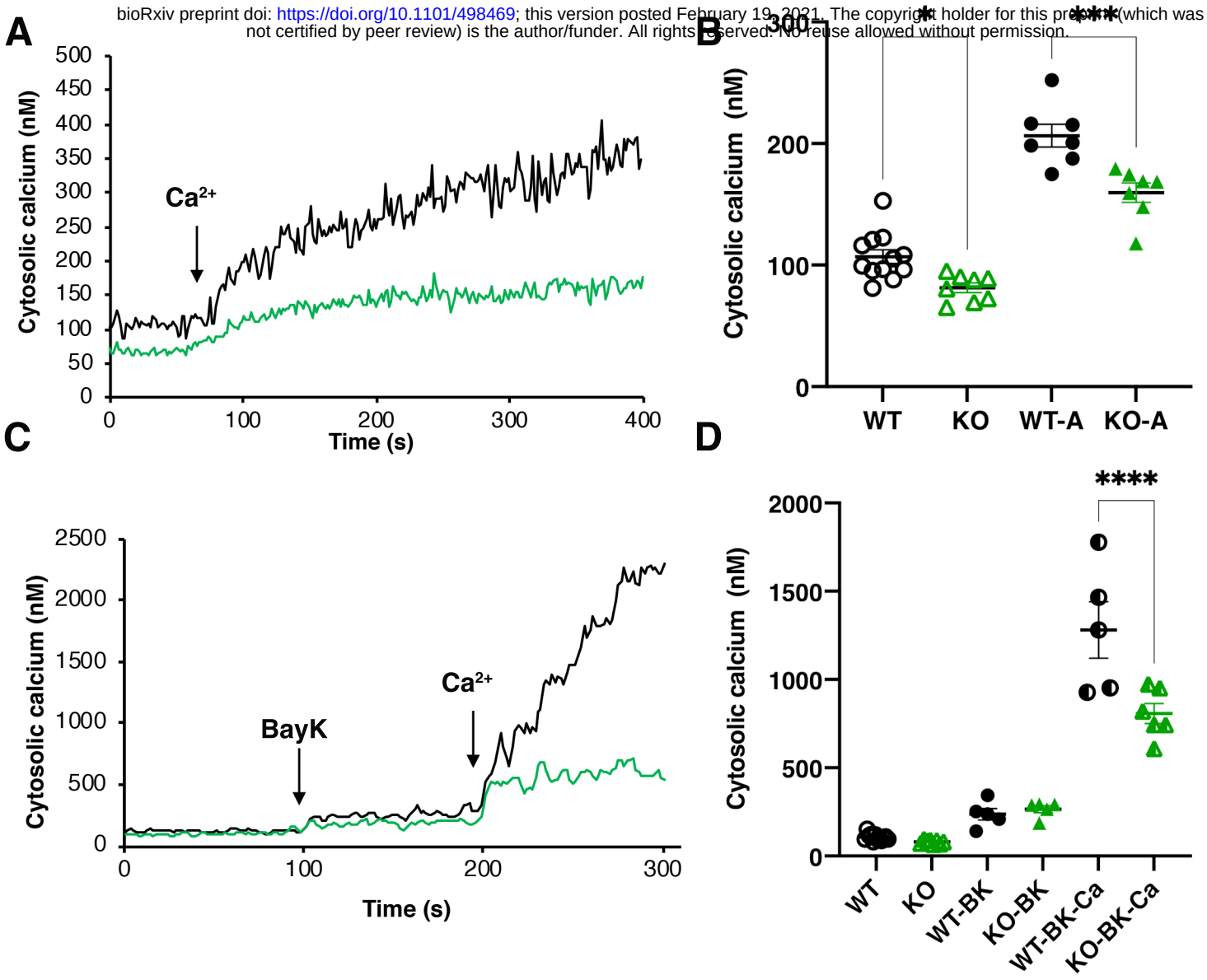

Fig. 7

bioRxiv preprint doi: https://doi.org/10.1101/498469; this version posted February 19, 2021. The copyright holder for this preprint (which was not certified by peer review) is the author/funder. All rights reserved. No reuse allowed without permission.

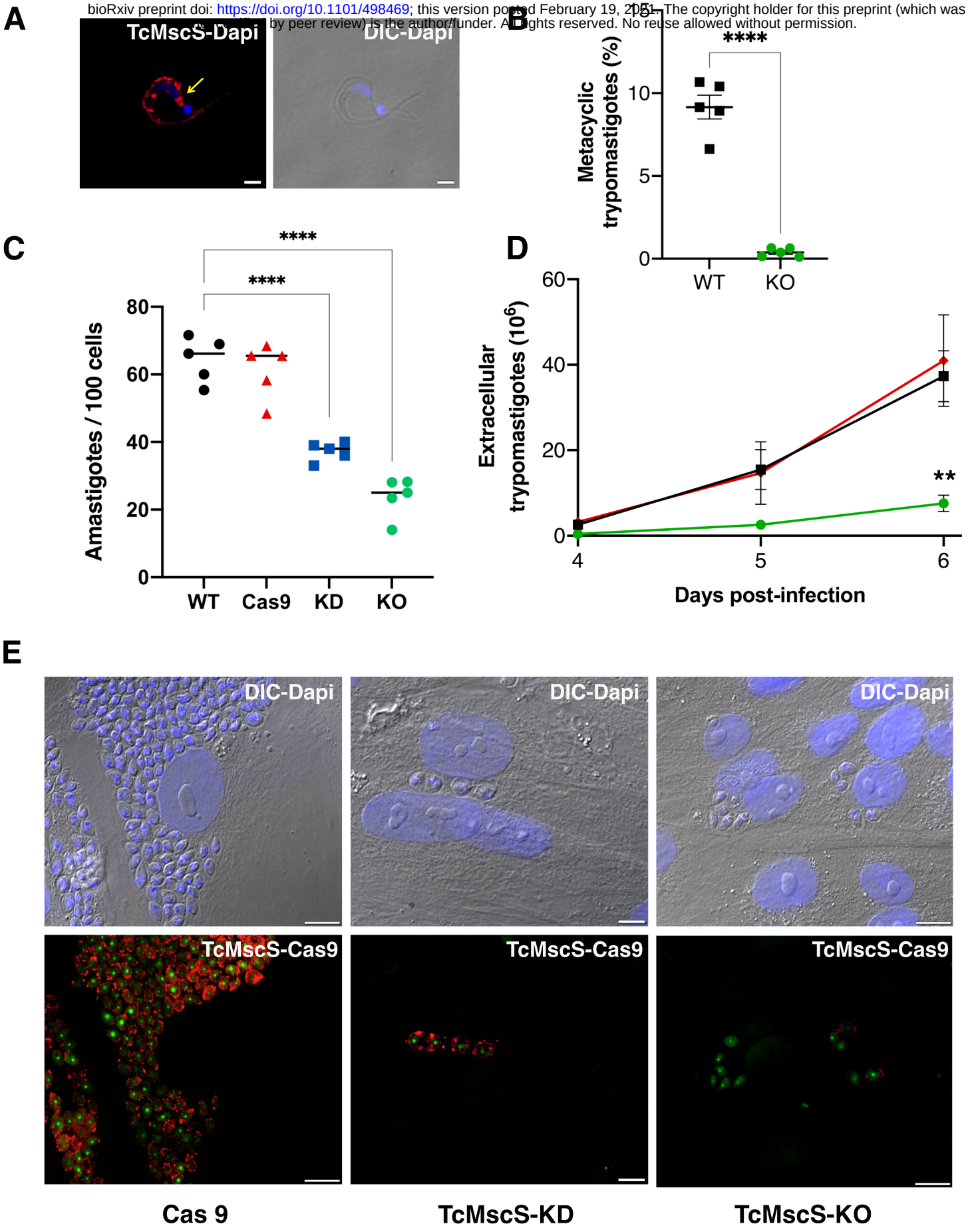

Fig. 8